ELSEVIER

Chemical Geology 208 (2004) 61–88

CHEMICAL GEOLOGY
INCLUDING
ISOTOPE GEOSCIENCE

www.elsevier.com/locate/chemgeo

Mantle formation and evolution, Slave Craton: constraints from HSE abundances and Re–Os isotope systematics of sulfide inclusions in mantle xenocrysts

Sonja Aulbach[a,*], William L. Griffin[a,b], Norman J. Pearson[a], Suzanne Y. O'Reilly[a], Kevin Kivi[c], Buddy J. Doyle[d]

[a] *Department Earth and Planetary Sciences, GEMOC ARC National Key Centre, Macquarie University, New South Wales, NSW 2109, Australia*
[b] *CSIRO Exploration and Mining, N. Ryde, NSW 2113, Australia*
[c] *Kennecott Canada Exploration Inc., 1300 Walsh Street, Thunder Bay, ONT., Canada P7E 4X4*
[d] *Kennecott Canada Exploration Inc., 354-200 Granville Street, Vancouver, BC, Canada V6C 154*

Abstract

Major elements, trace elements including highly siderophile elements (HSE) and Re–Os isotope ratios were analysed in situ on individual sulfide grains and one Fe metal grain enclosed in fresh xenocrystic olivine and pyroxenes from kimberlites in the Lac de Gras area, central Slave Craton. Reconstruction of low-temperature assemblages to high-temperature precursor sulfides shows that there are two major sulfide populations: nickeliferous monosulfide solid solution (mss), and a distinct group of S-deficient Ni- and Co-rich sulfides ($(Ni,Co,Fe)_{3-x}S_2$). The inclusion suite is unusual because all $(Ni,Co,Fe)_{3-x}S_2$, a subgroup of mss, and Fe metal inclusion have high W concentrations (up to 3400, 2600 and 24,000 ppm, respectively) and because $(Ni,Co,Fe)_{3-x}S_2$ have higher Ni and Co concentrations (mean 47 and 6.8 wt.%, respectively) combined with higher metal/sulfur (mean Me/S = 1.1) than the great majority of mantle-derived sulfides reported in the literature. Ca-in-olivine temperatures indicate that the host olivine and included sulfides are derived from the deep layer of the stratified lithosphere beneath Lac de Gras.

Re–Os isotope data were collected for 24 mss inclusions. $^{187}Re/^{188}Os$ ranges from 0.006 to 2.71, and $^{187}Os/^{188}Os$ from 0.1002 to 0.4732, corresponding to γ_{Os} from −21 to 272. The sulfides show a major mode of T_{RD} at ~2.8 Ga, extending to 3.9 Ga, and of T_{CHUR} at ~2.9 Ga. Eleven samples define an isochron at $t = 3.27 \pm 0.34$ Ga, with an enriched initial $^{187}Os/^{188}Os$ at t of 0.10725 ± 0.00014 ($\gamma_{Os,i} = 2.53 \pm 0.13$; MSWD = 0.75).

Weak covariations of Os contents and $^{187}Re/^{188}Os$ in mss with Mg/(Mg + Fe) of host olivine are consistent with variable degrees of melt depletion of sulfide-bearing peridotite. The incoherent behaviour of incompatible element abundances, the unrelated enrichment in the fluid-mobile elements W, As and Zn, and the unsupported radiogenic Os and recent Re-enrichment in some sulfides suggest repeated metasomatic processes subsequent to melting. The formation of the unusual $(Ni,Co,Fe)_{3-x}S_2$ could be related to metasomatism or alteration of mantle sulfide. However, the major element compositions of mss and $(Ni,Co,Fe)_{3-x}S_2$ would also be consistent with an igneous origin, by fractionation from extremely Ni-rich sulfide melts that unmix from S-bearing metal melts expected in the lower mantle.

Despite the evidence for interaction with fluids, some sulfides were able to preserve ancient melt-depletion signatures. Model ages and the isochron age in the deep lithosphere beneath Lac de Gras exceed the age of the overlying crust of the

* Corresponding author. Fax: +61-2-9850-8943.
E-mail address: saulb001@laurel.ocs.mq.edu.au (S. Aulbach).

0009-2541/$ - see front matter
doi:10.1016/j.chemgeo.2004.04.006

Contwoyto terrane. This "age paradox" may be reconciled if the lithospheric mantle beneath the adjacent older Central Slave Basement Complex (CSBC) was thrust beneath the younger Contwoyto terrane during collision of these two entities, resulting in a translithospheric northeast-dipping suture.

Keywords: Sulfide; HSE; PGE; Re–Os; Lithosphere; Slave Craton

1. Introduction

Monosulfide solid solution (mss) in mantle peridotites has compositions suggesting equilibrium with a sulfide melt (e.g., Craig, 1973) and commonly is interpreted as residual from partial melting (Helz, 1977; Lorand, 1987) or as crystallised from sulfide liquids trapped during partial melting (Mitchell and Keays, 1981; Hamlyn and Keays, 1986; Dromgoole and Pasteris, 1987). These sulfides are the main reservoir for highly siderophile elements (HSE) as well as other siderophile/chalcophile elements in the mantle (Mitchell and Keays, 1981; Garuti et al., 1984; Fleet and Stone, 1991; Pattou et al., 1996; Alard et al., 2000). Thus, the study of sulfides provides information additional and complementary to lithophile element studies on the silicate portion of the mantle.

Sulfide inclusions are expected to exchange Fe, Ni and Co with host olivine and pyroxenes (e.g., Thompson and Barnes, 1984), but should be shielded from exchange with external reservoirs with regard to trace elements that are incompatible in the host phase (Gaetani and Watson, 2000). The contents of PGE in the sulfides may therefore be protected from interaction with the kimberlite host or post-emplacement alteration, provided that the host silicates are not fractured during decompression in the ascending host magma (e.g., Lorand, 1990). Because olivine readily recrystallises in the mantle, e.g., during metasomatism (Drury and Van Roermund, 1989), sulfide inclusions may be subject to secondary overprints following their formation. A study of the major-element, trace-element and Os isotopic composition of sulfide inclusions should reveal whether the sulfide inclusions have remained shielded or interacted with external reservoirs. These data could then be used to understand pre-entrainment processes involved in the formation and evolution of the subcontinental lithospheric mantle.

For this purpose, olivine and pyroxene xenocrysts with sulfide inclusions were hand-picked from heavy-mineral concentrates of kimberlites at Lac de Gras, Slave Craton (Canada). The host silicates have compositions similar to minerals in peridotite xenoliths from the same locality (Pearson et al., 1999) and are interpreted as disaggregated mantle wall-rock. Sulfides, both enclosed and interstitial, have been identified in xenoliths from Lac de Gras (Pearson et al., 2002; authors' unpublished data), linking the xenocryst data of the present study to available xenolith data. In this contribution, we document the characteristics and composition of the sulfide inclusion suite, which includes Ni–Co-rich sulfides, examine their relationship to each other and propose models for their formation and implications for lithosphere formation in the central Slave Craton.

2. Geological setting

The material studied here consists of olivine and pyroxene grains separated from kimberlites, mostly the A154 pipe, in the Lac de Gras area, Slave Craton, Canada (Fig. 1). The Slave Craton is an amalgamation of terranes, including the ~4.0–2.7 Ga Central Slave Basement Complex (CSBC; Bleeker et al., 1999) in the west and the ~2.7 Ga arc-related Hackett River and Contwoyto terranes in the east (Kusky, 1989). Lac de Gras lies on the Nd isotopic line of Davis and Hegner (1992) and Davis (2003, personal communication), which separates rocks with Nd isotopic ratios indicative of ancient crust (west) from rocks with isotopic ratios indicative of juvenile sources (east). This line lies ~100 km east of the surficial suture between the CSBC and the Contwoyto Terrane into which the host kimberlites intruded, and has been interpreted as the leading edge of the CSBC at depth (Bleeker et al., 1999).

Using xenocryst and xenolith data from 18 kimberlites in the Lac de Gras area, Griffin et al. (1999) identified a shallow mantle layer that is ultra-depleted

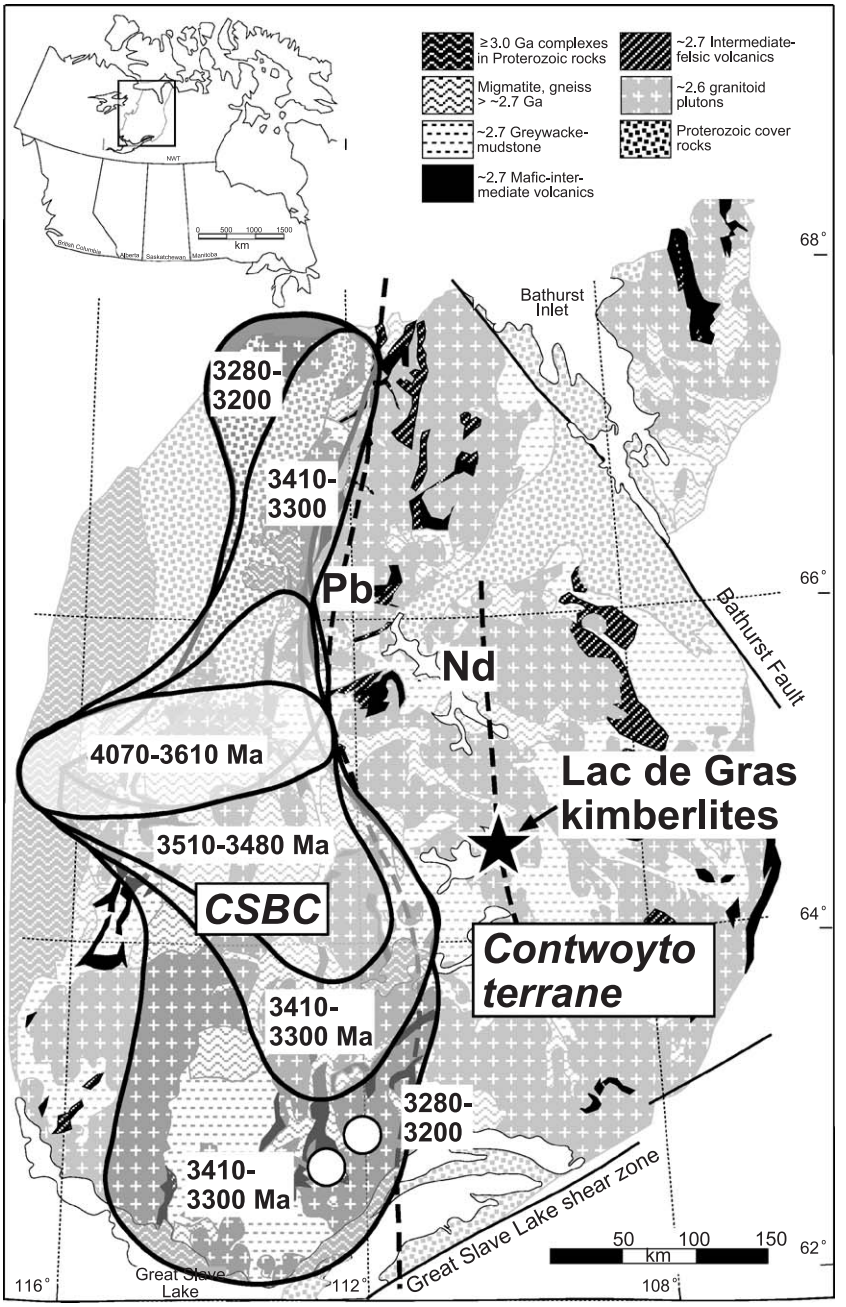

Fig. 1. Geological map of the Slave Craton after Padgham and Fyson (1992), with the location of the Lac de Gras kimberlites. Also shown are growth rings around an ancient core (Ketchum and Bleeker, 2001) in the CSBC (Central Slave Basement Complex; Bleeker et al., 1999), located in the western part of the Craton, and the Contwoyto terrane in the eastern part of the Craton. The Pb isotopic line of Thorpe et al. (1992, as quoted in: Pell, 1997) and the Nd isotopic line of Davis and Hegner (1992) and Davis (2003, personal communication) are shown for reference. Inset shows location within Canada.

in incompatible elements, which is separated by a sharp boundary at ~140 km from a moderately depleted deeper mantle lithosphere. The shallow layer compositionally resembles modern depleted abyssal peridotites and ophiolites from convergent margins, but has higher Mg- and Cr-numbers (Griffin et al., 1999). It may have formed in an arc setting, such as that suggested by Kusky (1989). The deeper layer is broadly similar to Archaean mantle worldwide, but trends toward lower Mg-numbers and higher olivine/orthopyroxene ratios than most Archaean sections (Gaul et al., 2000). Griffin et al. (1999) suggested that this deeper layer may have formed during underplating of a plume head or diapir that was moderately depleted by partial melting during ascent; this model is supported by the occurrence of diamonds containing lower mantle minerals (Davies et al., 1999).

3. Sample preparation and analytical techniques

Fifty two olivine grains, three orthopyroxene grains and one clinopyroxene grain containing sulfide inclusions, two discrete sulfide grains and one olivine containing a grain of Fe metal were hand-picked from coarse concentrate under the binocular microscope. Additionally, five grains of pyrite, three grains of pentlandite, and one grain each of pyrrhotite and chalcopyrite were retrieved from the olivine concentrate but are not reported here because they are not considered to be primary. All sulfides that were recognised were picked and prepared, i.e., no sampling criteria were applied. Samples were mounted individually in aluminium sleeves filled with epoxy and hand-polished using wet-and-dry sandpaper to expose the sulfide inclusion. A fine polish was obtained using a standard pellon polishing disk and diamond polishing paste.

Major-element contents were analysed using a CAMECA Camebax SX50 electron microprobe (EMP) in the GEMOC National Key Centre at Macquarie University (www.es.mq.edu.au/GEMOC/AnMethods/anmeth.html). Sulfide analyses were performed with an accelerating voltage of 20 kV, a beam current of 20 nA and a beam size of ≤3 μm. Counting times were 20 s on the peak and 10 s on each side of the background. The host silicates were analysed with a 15 kV acceleration voltage and counting times of 10 s on the peak and 5 s on the background. The PAP matrix correction procedure (Pouchou and Pichoir, 1984) was applied to the raw data. Bulk sulfide compositions were reconstructed by combining EMP analyses of the individual low-temperature phases with their modal abundances. Modes were calculated from X-ray element distribution maps (see Fig. 2) using an image analysis program (NIH Image 1.62 or ROCKMAS (in-house program by E. van Achterbergh)). Sometimes distinct exsolved phases were not evident in the X-ray maps. In this case, a traverse of analyses across the grain was averaged and this was taken as a representative composition.

Re–Os isotope data were collected with a Merchantek LUV266 laser microprobe attached to a Nu Plasma multi-collector ICPMS in the GEMOC National Key Centre at Macquarie University. Typical laser operating conditions are 4–5-Hz frequency, a beam energy of 2–5 mJ/pulse and 60–80-μm spot sizes. The higher beam energies were applied to large sulfide samples in order to increase the signal size. Two set-ups were used for collection of the ion beams: eight Faraday cups and Os as internal isotope standard for mass fractionation correction (sulfides C1–C43; $^{189}Os/^{192}Os = 0.39593$, Pearson et al., 2002), or a combination of eight Faraday Cups and two ion counters (for masses 185 and 187) and Ir (bled with Ar into the He gas carrying the ablated sample) as external mass fractionation correction (sulfides C78–C232). Drift on the ion counters was corrected for by bracketing sample analyses with analyses of standard PGE-A, a synthetic doped NiS bead with known Os isotopic composition. The overlap of ^{187}Re on ^{187}Os is corrected using ^{185}Re. The calibration procedures and the corrections applied as well as reproducibility of analyses of standard material are described in detail in the work of Pearson et al. (2002).

Some samples have low Os signals, which raises the question whether sufficiently accurate isotope data can be obtained from these samples. One way to test this is to compare measured to natural stable isotope ratios. Of 13 samples with Os signals <10 mV, 11 samples had 192/188 of 3.05 ± 0.11 (natural 3.08) and 190/188 of 1.94 ± 0.15 (natural 1.98). Two samples with deviating stable isotope ratios were discarded. The loss of precision at low signals is reflected in the increased within-run errors. Several samples (e.g., C78, C185) have very low analytical uncertainties

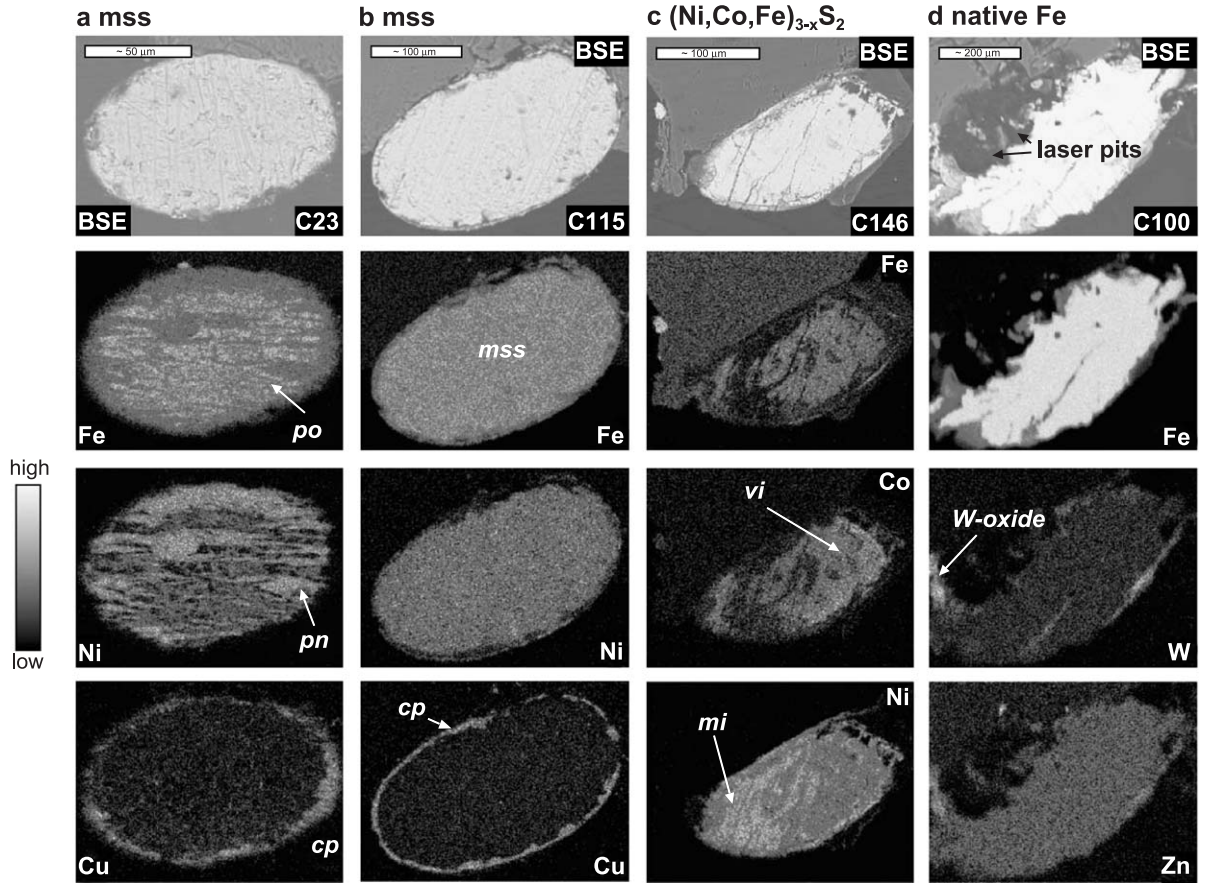

Fig. 2. Backscattered electron images (BSE, top row) and X-ray element distribution maps (second to bottom rows). Bright greys indicate high concentrations and dark greys indicate low concentrations (see bar at left). (a) Flame-like exsolutions of pyrrhotite (po) and pentlandite (pn) with chalcopyrite (cp) ring from assumed precursor monosulfide solid solution (mss); (b) mss with cp ring; (c) assumed precursor $(Ni,Co,Fe)_{3-x}S_2$ consisting of Co-rich violarite (vi) and Co-poor millerite (mi); (d) Fe metal with Zn-bearing W oxide.

on the measured $^{187}Re/^{188}Os$, reflecting unusually stable signals. Typical uncertainties on $^{187}Re/^{188}Os$ are at the percent level.

During Re–Os isotope analysis, 27 of the 58 sulfides (plus one Fe metal), including all 12 (Ni, $Co,Fe)_{3-x}S_2$, from Lac de Gras, showed anomalously high signals at mass 186. The contribution from ^{186}Os accounted for $\ll$1% of the total 186 signal and the signals point to a significant abundance of ^{186}W. W-rich samples, including all $(Ni,Co,Fe)_{3-x}S_2$, did not yield reliable Re and Os isotopic data because of scattering of the large W beam into the ion counters where masses 185 (for Re) and 187 (for ^{187}Os and ^{187}Re) were collected.

Trace-element data were collected from the sulfides left after LAM-MC-ICPMS analysis, using either a custom-built laser-ablation system (designed by S.E. Jackson) or a Merchantek LUV 266 Nd:YAG UV laser system, both linked to an Agilent 7500 ICPMS. The custom-built laser is a Continuum Surelite I-20 Q-switched quadrupled frequency (266 nm) Nd:YAG laser (Norman et al., 1996). Analyses consisted of 30–40 replicates (60 s) counted on the carrier gas for background subtraction and ~ 50 replicates on the sulfide grain (depending on the volume of material available). Ablation was done in an Ar atmosphere with a gas flow of 1.3 l/min, a repetition rate of 5 Hz and 0.5–1 mJ energy per pulse, and resulted in 40–

60-μm crater diameters. At these conditions, the Merchantek laser drills into the sample at about 1.4–1.2 μm/s (compared to about 1 μm/s for silicates at a repetition rate of 5 Hz; Jackson, personal communication). The relative sensitivity was calibrated against the in-house PGE-A NiS standard (to obtain Ru, Rh, Pd, Os, Ir, Pt, Au, As, Bi) and silicate glass standards NIST 610 or 612 (to obtain Zn, Mo, Ag, W and Re), using values of Jackson and Sharma (unpublished data) and Norman et al. (1996), respectively. Silicon, Ca and other lithophile elements were monitored to check if the host silicate phase was ablated in addition to the sulfide. Average abundances, standard deviations, 1σ errors and detection limits for the standard materials—analysed as unknowns—are given in Table 1. No differences were observed using the different laser systems.

The isotope ^{34}S was used as the internal standard for sulfides (^{65}Cu for the Fe metal inclusion) for the elements calibrated relative to PGE-A, a NiS-bead that is similar in matrix to sulfides. A $\pm$3% relative uncertainty on the S concentration determined by microprobe is propagated through all analyses. ^{62}Ni, derived from analysis relative to PGE-A, was used as the internal standard for all elements calibrated relative to the NIST glasses. The uncertainty on the Ni-content in PGE-A determined by ICPMS is $\sim$10% (Table 1). Mg concentration of olivine was determined by EMP and ^{24}Mg was used as internal standard for trace-element analyses of olivine. Raw data were processed on-line using the GLITTER software (Van Achterbergh et al., 1999; see http://www.es.mq.edu.au/GEMOC/glitter/).

Trace-element data collected by laser ablation may not always be representative of the bulk grain because most sulfides consist of polyphase low-temperature assemblages that were not necessarily ablated in modal proportions. While the variability and small anomalies in trace-element abundances probably reflect to a large degree the intrinsic heterogeneity of the samples, some variability could result from exsolution and/or diffusion-related grain-scale redistribution processes, combined with non-modal sampling. Because the chalcopyrite we analysed has distinctly higher S/Ni (avg 6.6) than mss (avg 2.0) or $(Ni,Co,Fe)_{3-x}S_2$ (avg 0.8), the over- and undersampling of exsolved chalcopyrite may be gauged by comparing bulk S/Ni (from microprobe and modal analysis) to S/Ni from trace-element analysis. Of 23 samples, ten have $(S/Ni_{bulk})/(S/Ni_{LAM})$ of 0.9 to 1.1, consistent with roughly modal

Table 1
Standard reproducibility (standards treated as unknowns)

PGE-A	Avg (ppm) (n=14)	Stdev	Avg 1 σ	mdl(ppm)
S	278,300	5200	11,000	171
Ni	770,000	72,000	54,000	0.7
Cu	253	25	16	0.16
As	143	12	8.7	0.9
Ru	249	34	22	0.064
Rh	265	36	23	0.032
Pd	279	28	19	0.036
Os	206	26	16	0.041
Ir	117	17	10	0.013
Pt	221	29	18	0.065
Au	251	23	16	0.043
Bi	244	26	13	0.035
NIST 610	**Avg (ppm) (n=10)**	**Stdev**	**Avg 1σ**	**mdl**
Si	339,000	26,000	14,000	52
K	466	47	15	1.5
Ca	82,000	9400	2600	59
Fe	461	27	15	5.1
Co	393	28	12	0.066
Ni	428	23	14	0.92
Cu	438	21	14	0.41
Zn	452	47	15	0.29
Mo	408	23	13	0.079
Ag	246	12	7.8	0.044
W	466	29	15	0.083
Re	61	22	2.0	0.039
NIST 612	**Avg (ppm) (n=5)**	**Stdev**	**Avg 1σ**	**mdl**
Si	314,000	16,000	23,000	22
K	81	19	3.3	0.97
Ca	81,300	9500	3000	17
Fe	52	1.0	2.3	2.1
Co	34	1.0	1.5	0.025
Ni	37	2.8	1.8	0.73
Cu	35	2.9	1.4	0.051
Zn	38	2.6	1.8	0.10
Mo	37	4.4	1.4	0.017
Ag	19	4.2	1.2	0.013
W	38	5.4	1.4	0.012
Re	8	1.3	0.31	0.0100

Average abundances determined by LAM ICPMS, standard deviations (stdev, external precision on repeat analyses), 1σ (within-run precision) and mean detection limits (mdl) for standards PGE-A, NIST 610 and NIST 612.

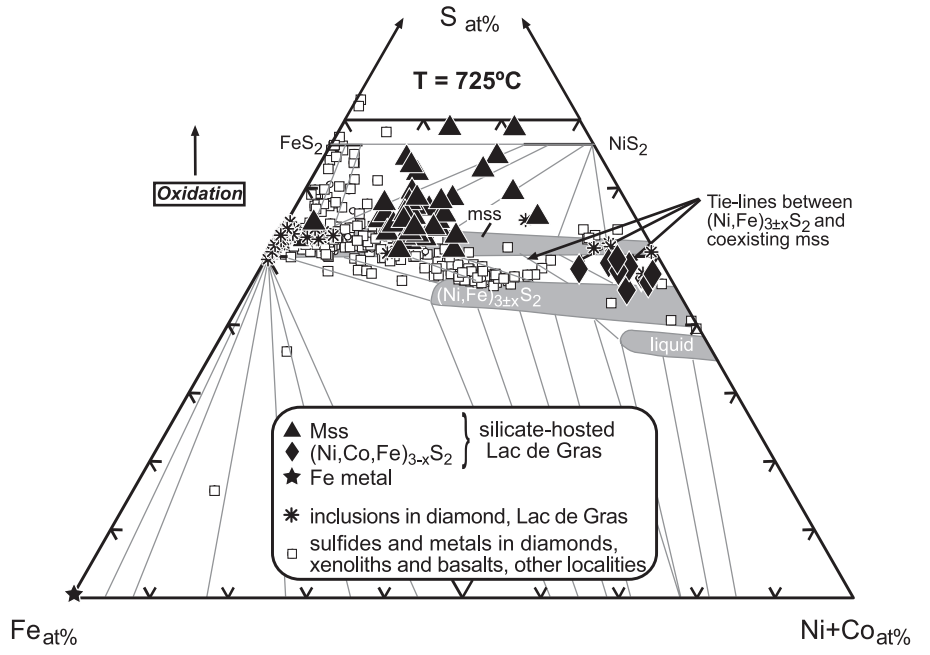

Fig. 3. The Fe–Ni–S system at 725 °C and ambient pressure (after Karup-Møller and Makovicky, 1995). Mss, $(Ni,Co,Fe)_{3-x}S_2$ and Fe metal from Lac de Gras are plotted against the fields of mss, $(Ni,Fe)_{3\pm x}S_2$ and liquid established by Karup-Møller and Makovicky (1995). Shown for comparison are sulfides occurring in basalts, pyroxenites, peridotites, olivine megacrysts and diamonds world-wide (Sobolev et al., 1981; Lorand and Conquéré, 1983; Garuti et al., 1984; Dromgoole and Pasteris, 1987; Lorand, 1987; Lorand and Ceuleneer, 1989; Fleet and Stone, 1990; Bulanova and Zayakina, 1991; Deines and Harris, 1995; Szabó and Bodnar, 1995; Roy-Barman et al., 1998; Davies et al., 1999, in prep.; Lorand and Alard, 2001; Richardson et al., 2001; Griffin et al., 2002).

sampling. For samples with higher or lower ratios, incompatible element variability may be related to a sampling bias. Three samples (C27, C74, C116) have $(S/Ni_{bulk})/(S/Ni_{LAM})$ outside the range of 0.8–1.2, suggesting a severe discrepancy between bulk sulfide composition and the composition sampled during

Table 2
Summary of assemblages and characteristics of concentrate mineral-hosted sulfides from Lac de Gras

Assemblages mss	mss	mss + cp	po + pn + cp	po + pn	mss + py	
n	5 (+1 dj)	26	8	5	1	
Assemblages $(Ni,Co,Fe)_{3-x}S_2$	$(Ni,Co,Fe)_{3-x}S_2$	$(Ni,Co,Fe)_{3-x}S_2$ + vi	$(Ni,Co,Fe)_{3-x}S_2$ + pn	pn + mi or gd	vi + mi or gd or hz	$(Ni,Co,Fe)_{3-x}S_2$ + cp
n	2	3	1	2	1 each	1
Grain sizes (μm)	>40	>100	>150	>200	>300	
n	23	17	7	8	3	
Shapes	elongate	spherical	polyhedral	irregular		
n	20	12	12	14		
Hosts	ol	opx	cpx	none		
n	52	3	1	2		

n = number of grains, cp = chalcopyrite, dj = djerfisherite, gd = godlevskite, mi = millerite, mss = monosulfide solid solution, pn = pentlandite, po = pyrrhotite, py = pyrite, vi = violarite; cpx = clinopyroxene, ol = olivine, opx = orthopyroxene.

Table 3
Major-element contents of reconstructed sulfides and Fe metal in wt.%

Sample	Mineral	Low-T assemblage	Host	Cu	Fe	Ni	Co	S	K	O	Total	%hem	M/S	Ni/(Ni+Fe)
C1	mss	mss, cp[a]	opx	11.05	36.32	11.68	0.69	33.47	<0.04	2.93	96.16	23.1	0.76	0.33
C3	mss	mss, cp[a]	ol	5.63	36.96	17.78	0.46	34.01	<0.04	2.26	97.10	16.6	0.82	0.39
C4	mss	mss, cp[b]	ol	7.07	37.37	15.52	0.34	35.43	<0.04	1.71	97.45	11.9	0.82	0.33
C19	alt mss	po, pn, cp	ol	8.15	35.39	12.29	0.31	29.77	<0.04	9.65	95.57	na	na	na
C20	mss	mss, cp[a]	ol	6.24	36.45	19.35	0.63	33.93	na	0.97	97.58	6.6	0.96	0.37
C21	mss	mss, cp[a]	ol	4.19	43.09	12.51	0.63	35.49	<0.04	1.43	97.34	8.3	0.85	0.25
C22	mss	mss, cp[a]	ol	3.48	32.99	18.96	0.29	33.41	na	5.51	94.64	63.6	0.49	0.71
C23	mss	po, pn, cp	ol	7.37	37.27	15.64	0.29	33.73	<0.04	2.02	96.33	14.4	0.84	0.35
C24	mss	mss, cp[a]	ol	5.92	39.02	13.82	0.39	34.72	<0.04	2.63	96.51	18.6	0.75	0.33
C25	mss	mss, cp[a]	ol	6.10	34.56	18.23	0.40	31.57	na	3.04	93.90	25.8	0.79	0.46
C26	alt mss	mss, cp[a]	ol	7.45	28.70	10.18	0.47	27.24	<0.04	8.74	82.78	na	na	na
C27	mss	mss, py[a]	ol	0.86	41.99	11.13	0.29	40.05	na	3.31	97.63	22.5	0.55	0.28
C38	mss	mss, cp[b]	ol	5.00	32.49	18.68	0.44	31.33	<0.04	4.63	92.58	49.7	0.61	0.62
C41	mss	mss, cp[b]	ol	2.77	39.13	19.87	0.46	34.48	<0.04	0.91	97.63	5.7	0.94	0.35
C42	mss	mss, cp[b]	ol	4.33	40.18	12.61	0.33	34.90	<0.04	1.32	93.68	8.3	0.82	0.26
C43	mss	mss, cp,alt[a]	ol	5.42	42.52	14.50	0.38	33.44	<0.04	2.00	98.28	12.3	0.89	0.29
C72	mss	po, pn, cp	ol	3.60	35.18	22.22	0.55	34.62	<0.04	1.42	97.59	10.4	0.89	0.43
C74	mss	po, pn	none	0.40	54.23	3.79	0.06	36.60	na	1.42	96.49	6.5	0.81	0.07
C78	mss	mss[b]	ol	1.39	36.91	23.13	0.50	37.14	na	0.50	99.57	3.3	0.90	0.39
C79	mss	mss, cp[a]	opx	3.07	40.19	18.53	0.36	34.82	<0.04	1.04	98.01	6.4	0.92	0.33
C80	mss	mss, cp[a]	ol	5.47	36.86	18.19	0.39	36.76	na	1.04	98.71	7.1	0.85	0.35
C83	altmss	po, pn, alt	ol	4.45	29.98	18.77	0.72	30.35	na	8.26	92.53	na	na	na
C85	mss	po, pn, cp	opx	5.97	34.90	19.70	0.47	32.67	<0.04	1.91	95.64	14.6	0.89	0.42
C100	Fe metal	Fe metal, Fe–W-oxide	ol	0.04	86.81	<0.07	<0.06	<0.08	na	3.56	93.45	na	na	na
C101	alt $(Ni,Co,Fe)_{3-x}S_2$	Ni-rich pn, mi, ~ hem	ol	4.20	10.23	37.22	1.26	22.85	na	18.17	93.92	na	na	na
C105	$(Ni,Co,Fe)_{3-x}S_2$	Ni-rich pn, gd	ol	0.78	14.58	47.50	2.44	30.83	na	1.59	97.72	33.9	1.03	0.86
C112	mss	mss, cp[a]	ol	13.07	37.55	11.19	0.24	34.11	na	1.28	97.45	8.6	0.91	0.25
C115	mss	mss, cp[a]	ol	3.76	40.66	14.58	0.35	34.64	na	2.61	96.59	17.5	0.76	0.33
C116	mss	pn, po	none	1.94	36.05	19.66	0.52	33.51	na	4.61	96.29	42.3	0.61	0.56
C120	alt $(Ni,Co,Fe)_{3-x}S_2$	$(Ni,Co,Fe)_{3-x}S_2$, FeO	cpx	0.78	8.37	50.16	3.04	31.16	na	3.99	97.49	na	na	na
C121	$(Ni,Co,Fe)_{3-x}S_2$	pn, $(Ni,Co,Fe)_{3-x}S_2$	ol	0.44	9.79	53.75	5.41	30.55	na	0.52	100.46	14.2	1.20	0.87
C122	$(Ni,Co,Fe)_{3-x}S_2$	vi, $(Ni,Co,Fe)_{3-x}S_2$	ol	0.71	10.41	43.79	11.55	31.80	na	1.21	99.47	37.0	1.05	0.90
C128	$(Ni,Co,Fe)_{3-x}S_2$	vi, $(Ni,Co,Fe)_{3-x}S_2$	ol	0.60	9.86	42.70	13.12	32.31	na	0.62	99.21	17.2	1.08	0.85
C130	$(Ni,Co,Fe)_{3-x}S_2$	vi,hz	ol	1.89	9.17	52.02	6.05	29.39	na	1.26	99.80	47.2	1.18	0.94
C132	alt $(Ni,Co,Fe)_{3-x}S_2$	cp, $(Ni,Co,Fe)_{3-x}S_2$	ol	0.48	2.18	57.00	3.59	27.60	na	5.82	96.66	na	na	na
C135	$(Ni,Co,Fe)_{3-x}S_2$	vi, $(Ni,Co,Fe)_{3-x}S_2$	ol	0.95	10.37	47.63	7.70	28.82	na	1.82	97.30	69.2	1.10	0.96
C140	$(Ni,Co,Fe)_{3-x}S_2$	$(Ni,Co,Fe)_{3-x}S_2$	ol	1.19	16.98	40.00	8.45	31.80	na	0.99	99.41	15.6	1.07	0.75
C143	alt $(Ni,Co,Fe)_{3-x}S_2$	vi, gd	ol	0.18	4.39	49.05	8.22	29.93	na	4.61	96.38	na	na	na
C146	$(Ni,Co,Fe)_{3-x}S_2$	vi, mi	ol	1.44	10.49	42.79	11.29	33.15	na	0.96	100.12	27.0	1.02	0.87
C156	mss	po, pn, cp	ol	2.45	34.24	25.24	0.46	33.72	<0.04	1.65	97.75	12.6	0.91	0.47
C158	mss	mss, cp[b]	ol	5.47	39.74	15.29	0.35	34.61	<0.04	1.91	97.37	12.6	0.84	0.32
C159	mss	po, pn, cp	ol	2.10	36.35	20.36	0.59	33.66	<0.04	2.45	95.51	18.6	0.80	0.44

Table 3 (*continued*)

Sample	Mineral	Low-T assemblage	Host	Cu	Fe	Ni	Co	S	K	O	Total	%hem	M/S	Ni/(Ni+Fe)
C171	mss	mss, cp[a]	ol	6.57	24.15	31.85	1.05	32.39	<0.04	2.52	98.56	32.1	0.88	0.71
C173	mss	po, pn, cp	ol	10.35	32.74	17.84	0.39	32.71	0.76	2.13	96.91	17.8	0.86	0.43
C174	mss	po, pn	ol	0.95	34.51	27.83	0.61	34.79	<0.04	0.96	99.65	6.9	0.96	0.47
C175	mss	po, pn, cp	ol	1.35	30.02	24.25	0.61	30.96	0.18	3.80	91.07	41.7	0.69	0.65
C185	mss	mss, cp[a]	ol	9.59	36.96	11.11	0.51	32.86	<0.04	4.94	96.01	45.2	0.58	0.43
C186	mss	mss[a]	ol	2.03	31.10	8.62	0.31	27.58	<0.04	2.69	72.34	25.2	0.60	0.31
C205	mss	mss, cp[b]	ol	3.94	40.12	18.33	0.40	34.21	<0.04	1.53	98.56	9.8	0.91	0.35
C206	mss	mss, cp[a]	ol	6.11	41.18	11.98	0.34	33.89	<0.04	1.70	95.23	10.7	0.85	0.26
C211	alt mss	alt mss, cp[a]	ol	5.08	21.58	9.20	0.28	19.67	<0.04	8.56	64.40	na	na	na
C216	mss	mss, cp[a]	ol	3.88	37.50	14.79	0.31	33.56	<0.04	2.47	92.52	18.1	0.75	0.35
C217	mss	mss, cp[b]	ol	3.57	42.29	15.04	0.60	34.96	<0.04	1.12	97.59	6.6	0.90	0.28
C226	mss	mss, cp[b]	ol	5.75	39.06	16.12	0.36	35.04	<0.04	1.43	97.77	9.3	0.87	0.32
C229	alt dj	dj	ol	1.92	28.41	18.51	0.62	28.21	2.99	9.13	89.79	na	na	na
C230	mss	po, pn	ol	<0.06	42.44	20.01	0.72	36.15	<0.04	0.56	99.92	3.2	0.95	0.32
C231	mss	mss[a]	ol	1.30	35.67	23.27	0.44	37.79	<0.04	0.83	99.31	5.7	0.84	0.41
C232	mss	mss[a]	ol	0.76	32.37	21.51	0.71	32.03	<0.04	0.96	88.34	7.4	0.89	0.42
C233	mss	mss[b]	ol	2.02	38.58	20.15	0.44	37.57	<0.04	0.86	99.62	5.5	0.85	0.36

Sulfides were reconstituted from analyses of low-temperature phases; low-T = low-temperature; M/S = metal/sulfur; alt = altered; na = not analysed or not available; other abbreviations as in Table 2; oxygen is thought to be present due to oxidation and %hem denotes the percentage of Fe that may be tied up with oxygen in hematite; (M/S) and Ni/(Ni + Fe) calculated from atomic proportions (after subtraction of O and Fe as hematite; not given where more oxygen was present than could be subtracted with the available Fe = altered sulfides).

[a] Weak mottled variations in Ni-content.

[b] Weakly Ni-richer outer rings or cores.

laser ablation. The trace-element data for these three samples are not reported here.

4. Sulfide mineralogy and chemical composition

Images obtained using energy-dispersive spectrometry show that most sulfides consist of multiple phases, with varying S, Fe, Co and Ni content (Fig. 2a–c). Based on the rounded or polygonal shape of the sulfide grains, their internal structure and the compositions of coexisting phases, we interpret the multi-phase sulfide inclusions in xenocrystic olivine, orthopyroxene and clinopyroxene as low-temperature assemblages that exsolved from single high-temperature solid solutions upon cooling, during eruption of the host kimberlite (cf. Lorand, 1990). Pre-exsolution compositions were calculated from low-temperature assemblages as described in Section 3. Altogether, estimates were made of the composition of 45 Fe-rich monosulfide solid solution grains (mss, Fe/Ni>1), an unusual population of 12 Ni- and Co-rich grains, 1 grain of djerfisherite and 1 grain of Fe metal.

4.1. Reconstructed monosulfide solid solution (mss)

Precursor mss could in some cases be identified by their microstructure and, more commonly, by their bulk composition, which plots in the mss-field of Craig (1973) at 300 °C. To distinguish mss from pyrrhotite (po), a cut-off of 5 wt.% Ni was applied, corresponding to the maximum solubility of Ni in the po structure (Cabri, 1973). Only sample C74 has Ni <5 wt.% and, considering the compositional gap in Fe/Ni between this sample and other sulfides, it probably represents a pyrrhotite. Only 13 of the 45 reconstructed mss show typical exsolved flames of pentlandite in pyrrhotite (Fig. 2a). More often, only weakly inhomogeneous distribution of Ni in the grain was recognised, which was either flame-like or mottled, or visible as weakly Ni-rich rings and, rarely, as Ni-rich cores (Fig. 2b). Chalcopyrite occurs mostly as thin rims (in near-median sections), and subordinately as streaks throughout the sulfide grain. Cross-sections of the silicate-enclosed sulfide grains range from spherical to elongate to subangular polyhedral. Sulfide assemblages and modes, host phases, grain sizes and shapes are summarized in Table 2.

The major-element compositions of the sulfides are listed in Table 3. The high oxygen contents in some sulfides exceed the solubility of this element in the sulfide structure, particularly at mantle pressures (Wendlandt, 1982; Mavrogènes and O'Neill, 1999). Therefore, oxygen was subtracted by calculating and extracting a hypothetical iron oxide (Fe_2O_3) in order to calculate metal–sulfur ratios (M/S) and Ni/(Ni + Fe). Where more oxygen was present than could be removed with the available Fe content, sulfides are designated as altered, and no M/S or Ni/(Ni + Fe) is given. Major-element analyses were not normalised to 100, to give a more faithful reflection of the measured major-element contents.

Fig. 3 shows the calculated composition of the sulfides in the Fe–S–(Ni + Co) quadrilateral. Ni/(Ni + Fe) ratios in mss range from 0.25 to 0.71 (0.07 for pyrrhotite), with Ni contents of 8.6 to 31.9 wt.%. Metal/sulfur ranges from 0.49 to 0.96; most values are >0.8 (Fig. 4). Copper and Co contents range from < 0.06 to 13.1 wt.% and from 0.06 to 1.1 wt.%, respectively. Oxygen contents are generally below 6 wt.%, but may be as high as 9.7 wt.%. The presence of oxygen may be associated with the breakdown (e.g., oxidation) of sulfide. Despite the high oxygen contents observed in some mss, no discrete alteration products, such as magnetite, have been observed. The oxygen is assumed to be present as submicroscopic magnetite exsolutions that are not resolvable by EMP analysis, rather than residing in the sulfide lattice.

Trace-element data were collected for 16 of the mss grains (Table 4). Mss may contain up to hundreds of ppm of Mo, Ru, Ag, Os, Ir and Pt, and < 100 ppm of Rh and Pd, while As, Au and Bi are present at a level < 10 ppm. Zn is the most abundant of the trace elements, with concentrations ranging from below

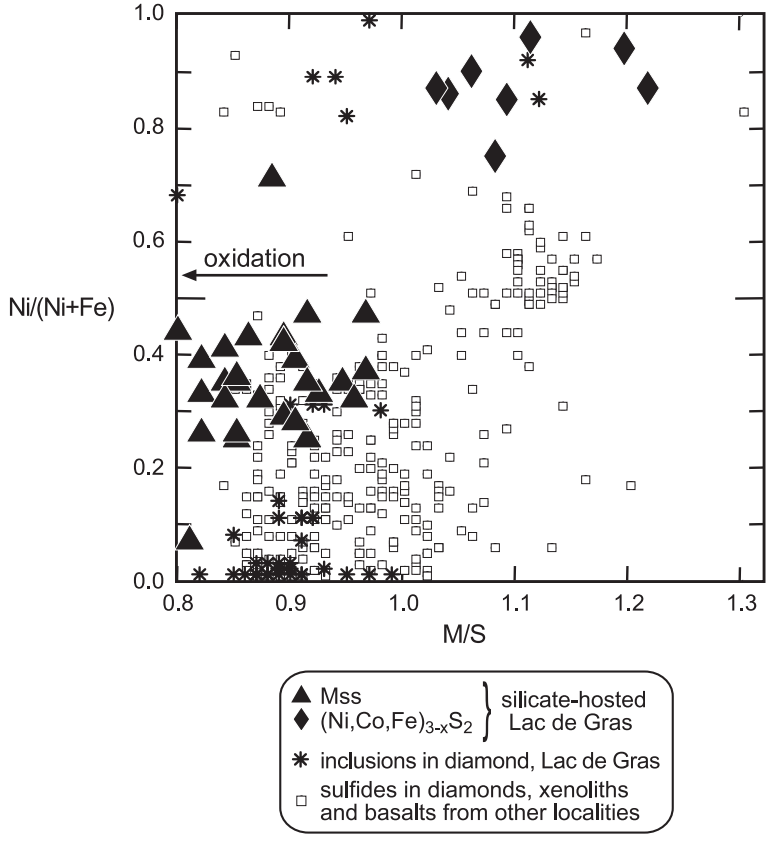

Fig. 4. Metal/sulfur (M/S) versus Ni/(Ni + Fe) for sulfides from Lac de Gras and from other localities (references as in Fig. 3); the removal of Fe with oxygen during oxidation leads to lower M/S than shown here, as indicated by the arrow.

Table 4
Trace-element abundances of sulfides in ppm

Sample	Mineral	Zn	As	Mo	Ru	Rh	Pd	Ag	W	Re	Os	Ir	Pt	Au	Bi
C1	mss	42	0.45	12.2	370	65	0.22	3.5	4.1	0.24	280	162	0.51	0.104	1.6
1σ		2	0.08	0.9	20	3	0.02	0.2	0.3	0.03	20	12	0.04	0.010	0.1
C4	mss	4500	2.4	105	15.4	1.69	4.3	8.9	1.1	0.47	5.2	3.0	8.7	0.07	73
1σ		200	0.5	9	0.8	0.1	0.2	0.7	0.1	0.07	0.4	0.3	0.6	0.03	5
C19	mss	1210	1.4	35	1.34	0.21	4.17	210	0.11	0.24	1.18	0.41	2.95	0.16	4.3
1σ		70	0.1	3	0.08	0.01	0.2	20	0.02	0.03	0.10	0.04	0.22	0.02	0.3
C22	mss	31		10.7	6	1.3	12	5.0	0.62	1.52	3.2	1.59	7	0.23	4.5
1σ		2		0.4	2	0.4	3	0.8	0.03	0.06	0.7	0.4	2	0.04	0.2
C23	mss	700		57	11	0.7	5	7	0.4	0.60	14	9	5	0.12	0.9
Stdev/1σ	(*n* = 2)	300		2	4	0.3	1	1	0.2	0.03	4	3	1	0.03	0.3
C41	mss	125	2.1	31	31	3.8	12.4	1.1	0.024	0.48	27	13	4.7	0.028	< 0.03
1σ		9	0.1	4	2	0.3	0.7	0.1	0.006	0.07	3	2	0.5	0.004	
C42	mss	< 40		39	2.2	0.05	0.06	2.1	< 0.01	0.012	0.8	0.365	0.10	< 0.014	0.27
Stdev/1σ	(*n* = 2)			1	0.9	0.02	0.02	0.4		0.005	0.2	0.14	0.03		0.07
C43	mss	63		21	30	4	6	10	< 0.01	0.95	10	5	2.3	0.03	9
Stdev/1σ	(*n* = 2)	40		3	10	2	2	2		0.05	4	2	0.8	0.01	2
C85	mss	62	10.3	15.2	60	6.6	1.4	5.2	790	< 0.07	65	47	160	0.1	0.4
1σ		4	0.7	0.8	4	0.5	0.1	0.3	30		4	3	10	0.0	0.0
C100	Fe metal	68	93	24	< 0.07	0.072	< 0.05	6.8	24,000	0.3	< 0.03	< 0.02	< 0.072	0.1	0.1
1σ		5	6	1		0.03		0.4	1000	0.1				0.0	0.0
C112	mss	50	3.9	28	65	6.2	0.7	2.5	1720	0.1	17	8.9	6.3	0.1	0.0
1σ		3	0.3	1	5	0.5	0.1	0.1	60	0.0	1	0.6	0.5	0.0	0.0
C120	$(Ni,Co,Fe)_{3-x}S_2$	57	3.5	11.9	15	0.99	0.79	3.8	280	0.14	4.3	3.2	0.40	0.041	4.0
1σ		4	0.3	0.7	1	0.08	0.06	0.2	9	0.01	0.3	0.2	0.04	0.007	0.4
C128	$(Ni,Co,Fe)_{3-x}S_2$	1300	9.3	54	850	81	9.2	3.83	3100	1.20	160	102	2.7	0.21	0.33
1σ		100	0.6	3	60	6	0.6	0.2	100	0.06	10	7	0.2	0.02	0.03
C130	$(Ni,Co,Fe)_{3-x}S_2$	58	1.9	8.7	28	3.6	3.0	31	73	0.50	35	15	1.8	0.10	0.041
1σ		5	0.2	0.5	2	0.3	0.2	2	2	0.03	2	1	0.2	0.01	0.007
C146	$(Ni,Co,Fe)_{3-x}S_2$	7.7	2.9	42	9	1.4	30	1.3	3400	0.42	7	3	4	0.18	0.20
1σ		0.7	0.3	1	4	0.7	10	0.3	100	0.02	3	1	2	0.06	0.02
C173	mss	66	7.8	20.9	1.9	0.10	2.2	0.51	2600	0.42	0.63	0.31	1.0	0.08	0.022
1σ		8	0.5	0.7	0.2	0.03	0.2	0.05	100	0.03	0.07	0.03	0.1	0.02	0.010
C205	mss	14	0.54	19.8	13	1.7	7.7	1.6	0.11	0.40	4.4	2.6	2.4	0.03	0.014
1σ		2	0.10	0.7	1	0.1	0.7	0.2	0.02	0.03	0.4	0.2	0.2	0.01	0.005
C216	mss	14	0.32	28.8	4.7	0.71	11.8	0.52	< 0.03	1.32	2.7	1.2	13	0.08	0.044
1σ		2	0.09	0.9	0.4	0.06	1.0	0.05		0.05	0.2	0.1	1	0.01	0.006
C226	mss	19	0.38	46	4.8	0.52	0.36	0.29	0.03	0.16	3.4	2.1	0.38	< 0.01	0.58
1σ		3	0.08	2	0.4	0.05	0.04	0.04	0.02	0.02	0.3	0.2	0.04		0.03
C231	mss	19	2.3	56	59	11.9	31	1.9	0.06	1.63	57	29	61	1.4	0.65
1σ		3	0.2	2	5	1.0	3	0.2	0.02	0.07	4	2	5	0.1	0.04
C233	mss	20	1	16.0	9.0	1.00	21	3.3	0.18	1.59	4.7	2.5	19	17	3.5
1σ		3	0	0.6	0.8	0.09	2	0.3	0.03	0.08	0.4	0.2	2	1	0.2

Stdev = standard deviation (in italics), 1σ = one sigma error (within-run precision); where several analyses of the same grain were available, the larger of the two errors is given; na = not available; other abbreviations as in Table 2.

detection (0.10–0.29 ppm) to 4500 ppm. W abundances range from below detection (0.01 to 0.08 ppm) to 2600 ppm.

We have grouped samples without W-enrichment into those with high Pd/Ir relative to the primitive mantle (Pd/Ir_{PM}, = 1.2, values of McDonough and Sun, 1995) and those with lower Pd/Ir. We use the normalisation to primitive mantle (indicated by the suffix $_{PM}$) because the HSE budget of peridotite is contained within sulfide (e.g., Pattou et al., 1996; Alard et al., 2000), and the pattern obtained after normalisation should make fractionation evident. Samples with $Pd/Ir_{PM} < 1$ (Fig. 5a) have a weak to marked negative slope from the compatible IPGE (iridium

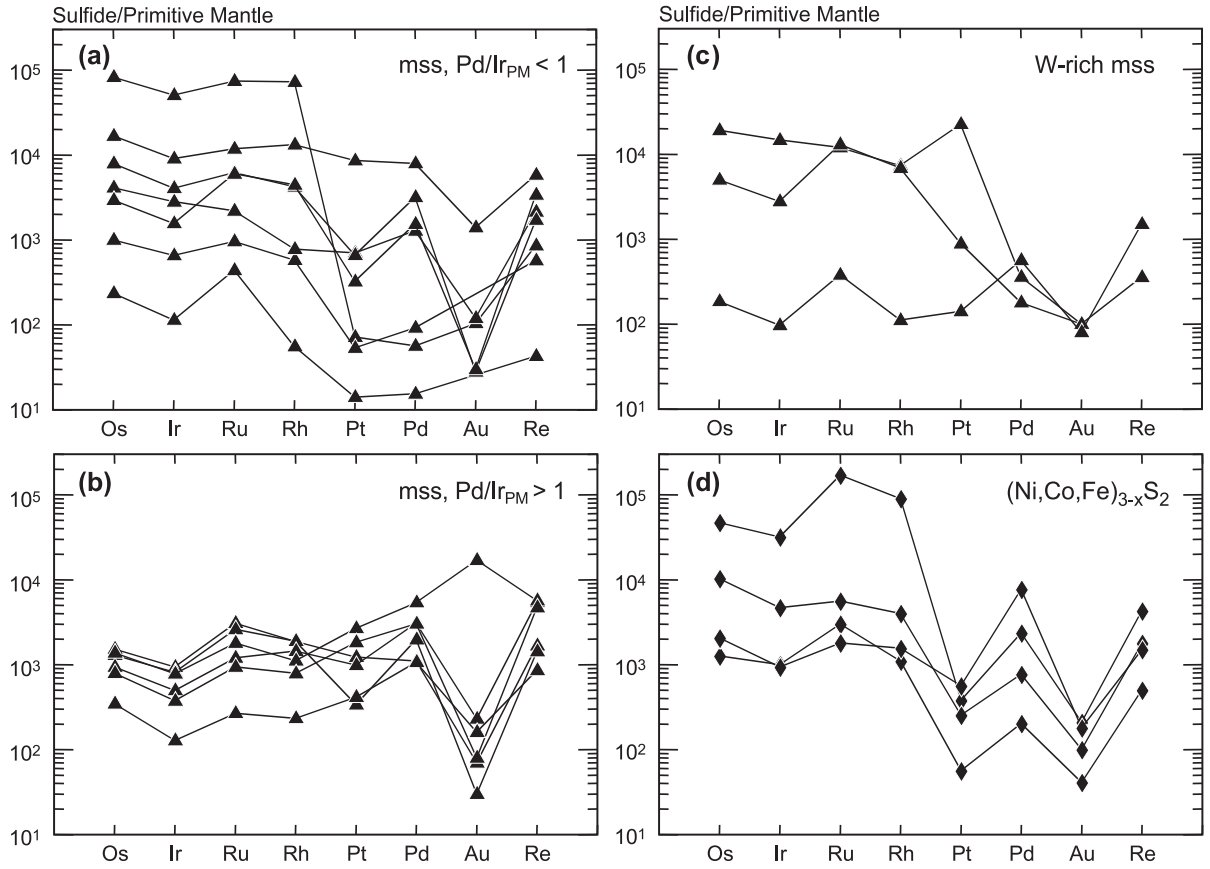

Fig. 5. Extended PGE patterns of (a) mss with chondrite-normalised Pd/Ir (Pd/Ir$_{PM}$)>1 and (b) with Pd/Ir$_{PM}$ < 1, (c) W-rich mss and (d) (Ni,Co,Fe)$_{3-x}$S$_2$. Normalised to primitive mantle of McDonough and Sun (1995).

group: Ru, Os, Ir) to the incompatible PPGE (palladium group: Rh, Pd, Pt) and Au. Four of these samples have negative Pt anomalies. Re abundances are mostly similar to those in samples with Pd/Ir$_{PM}$>1. The range of PGE abundances is large, with IPGE$_{PM}$ ranging from ~ 10^2 to 10^5 and PPGE$_{PM}$ from 10 to 10^4. Samples with Pd/Ir$_{PM}$>1 (Fig. 5b) have PGE$_{PM}$ ~ 100–5000, a weak positive slope from the IPGE to the PPGE, and Au$_{PM}$, ≤300, with the exception of sample C233 which is enriched in Au$_{PM}$, relative to Re$_{PM}$ and Pd$_{PM}$. Two of the samples have negative Pt anomalies. Three W-rich samples (Fig. 5c) have disparate IPGE abundances, with comparatively low Pd$_{PM}$ and nearly uniform Au$_{PM}$. One sample (C173) has Pd/Ir$_{PM}$>1, with a PGE pattern resembling those in Fig. 5a. A second sample (C85) has smoothly decreasing PGE$_N$ with the exception of a positive spike in Pt, and a third sample (C112) with Pd/Ir$_{PM}$ < 1 has a PGE pattern resembling those in Fig. 5b.

4.2. An unusual sulfide phase: Ni–Co-rich sulfides ((Ni,Co,Fe)$_{3-x}$S$_2$)

Ni–Co-rich sulfides have a streaky, mottled, concentric or fishnet-like appearance or combinations thereof as a result of the distribution of major elements (Fig. 2c). In most cases, the average analyses for Ni-poor phases showed higher NiO contents and averages for Ni-rich phases showed lower NiO contents than the pure endmember compositions. Upon exsolution, Co is partitioned into the Ni-poorer of the coexisting phases, with the exception of sample C101 which consists of Co-rich millerite and Co-poor altered (>20 wt.% O) pentlandite. The assemblage

of Ni–Co sulfide plus cp is clearly at disequilibrium (see phase relations in the work of Craig, 1973).

Like nickeliferous mss, which has the structural formula $Fe_{1-x}S$, reconstructed bulk Ni–Co-rich sulfides are non-stoichiometric and may be described as $(Ni,Co,Fe)_{3-x}S_2$. They compositionally partially overlap with sulfide in equilibrium with mss and residual liquid in the Fe–Ni–S system (see Fig. 3); this sulfide appears on the liquidus at 862 °C and atmospheric pressure (Kullerud et al., 1969; Karup-Møller and Makovicky, 1995). $(Ni,Co,Fe)_{3-x}S_2$ have Ni/(Ni+Fe) ratios from 0.75 to 0.96, and they plot below the mss field in Fig. 3. M/S ratios are higher than for mss, ranging from 1.02 to 1.20. Copper and Co contents range from 0.2 to 4.2 wt.% and 1.3 to 13.1 wt.%, respectively. Oxygen contents are variable between 0.5 and 18.2 wt.% and are probably related to the alteration of the sulfide. Discrete alteration products observed with $(Ni,Co,Fe)_{3-x}S_2$ are FeO in sample C120 and a phase approaching hematite composition in sample C101. These phases were not considered in reconstruction of single high-temperature precursor sulfides. Other high-Ni samples with high O contents (C132, C140) do not show discrete alteration phases, which may be present at the submicroscopic level. Fig. 4 shows that mss inclusions from Lac de Gras are broadly similar to sulfide suites from other localities. In contrast, $(Ni,Co,Fe)_{3-x}S_2$ occupies a compositional field at high Me/S and Ni/(Ni+Fe) that is not overlapped by the vast majority of sulfides in basalts and in mantle-derived pyroxenites, peridotites, olivine megacrysts and diamonds from other localities world-wide.

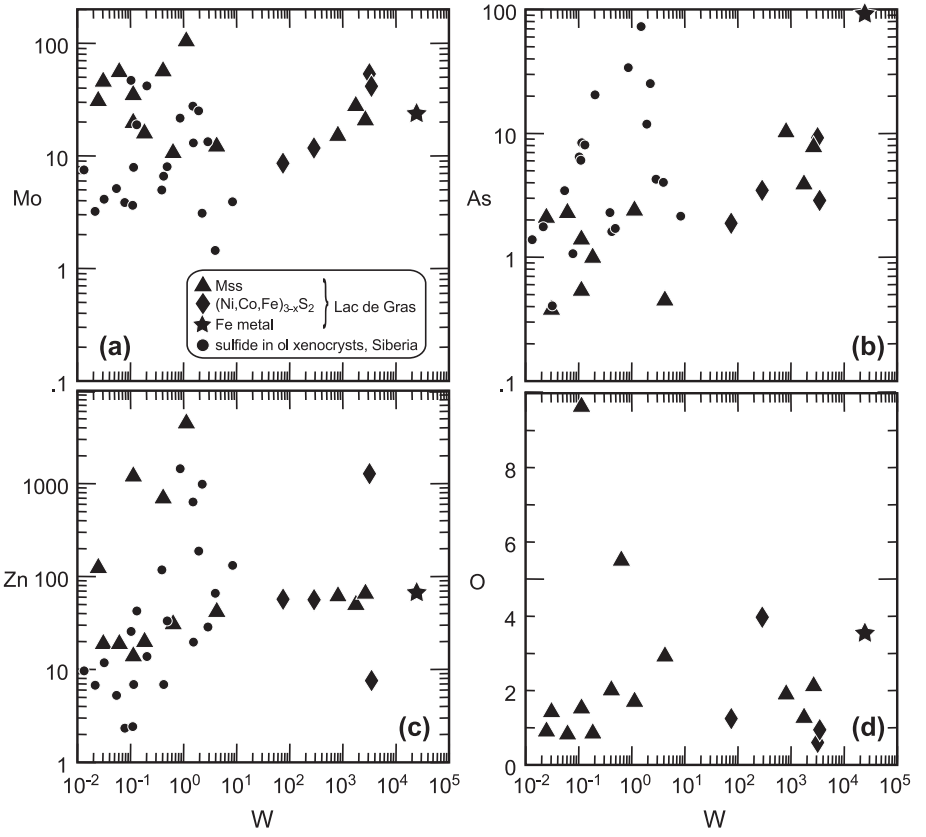

Fig. 6. W (ppm) versus a) Mo (ppm), b) As (ppm), c) Zn (ppm) and d) O (wt.%). Shown for comparison are sulfide inclusions in olivine xenocrysts from Siberia (Griffin et al., 2002).

Trace-element data were collected for four of the $(Ni,Co,Fe)_{3-x}S_2$ (Table 4). Ru, Os and Ir abundances in $(Ni,Co,Fe)_{3-x}S_2$ are up to hundreds of ppm. Mo, Rh, Pd and Ag can have abundances in the tens of ppm, while As, Re, Pt, Au and Bi are present at concentrations <10 ppm. One sample has a high Zn content of 1,300 ppm. W reaches concentrations in the thousands of ppm. Three of the four samples have $Pd/Ir_{PM}<1$ (Fig. 5d). The $(Ni,Co,Fe)_{3-x}S_2$ with the highest IPGE abundances has unusually high Rh/Ir and Ru/Ir. All four $(Ni,Co,Fe)_{3-x}S_2$ have negative Pt anomalies.

4.3. Fe metal trace-element composition

Analysis of the Fe metal grain by EMP yielded W concentrations between 0.1 and 30.8 wt.%, which indicates that W is not homogeneously distributed in the grain. This is also evident from Fig. 2d. Domains of high W abundances are associated with high Zn and oxygen contents and represent discrete W-bearing Fe oxide and Fe-bearing W oxide with approximately hematite stoichiometry. The two oxide phases cannot be discerned in Fig. 2d, but represent significantly distinct groups of EMP analyses obtained from the W-rich domain. The bulk composition in Table 3 was tentatively reconstructed from 80% Fe metal, and 10% each of W–Fe oxide and Fe–W oxide. Analysis by LAM ICPMS yielded 24,000 ppm W and an Fe content of 86 wt.%, which may be close to the bulk composition. Higher W abundances in the metal compared to sulfides are consistent with the siderophile character of W (Jana and Walker, 1997). While absolute trace-element abundances in the Fe metal suffer from uncertainties in the reconstructed bulk composition, relative abundances are considered to be robust. The most striking characteristics of Fe metal trace-element abundances are the distinct negative Co and Ni anomalies and positive W anomaly relative to elements of similar siderophile character (not shown).

4.4. W-enrichment

All $(Ni,Co,Fe)_{3-x}S_2$, some of the mss and the Fe metal inclusion have high W contents (up to 3400,

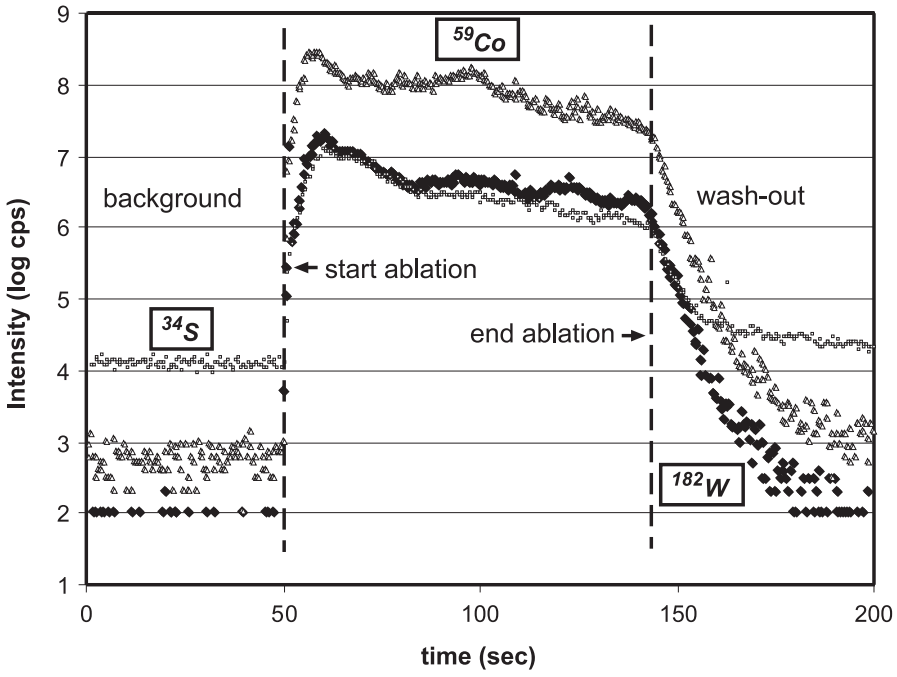

Fig. 7. Time (in seconds) versus intensity (raw counts per second) during quadrupole ICPMS analysis. Results for ^{34}S (squares), ^{59}Co (triangles) and ^{182}W (diamonds) are shown.

2600 and 24,000 ppm, respectively). Tungsten is a highly refractory, moderately siderophile element with similar chemical properties to Mo (Lodders and Palme, 1991; Ertel et al., 1996). These two elements are correlated in the high-W sulfides (W ≥ 10 ppm) (Fig. 6a). Arsenic is the only element for which the average content in high-W sulfides is higher than that in low-W sulfides, but there is no correlation between W and As in high-W sulfides (Fig. 6b). Likewise, there is no correlation with Zn, another element for which unusual enrichments are observed in some sulfides (Fig. 6c). Tungsten is also not correlated with either compatible or incompatible HSE.

There are several arguments why the high W-contents observed for all of the $(Ni,Co,Fe)_{3-x}S_2$ and 28%

Table 5
Re–Os isotope compositions and model ages

Sample	$^{187}Re/^{188}Os$	±	$^{187}Os/^{188}Os$	±	Reference[a]	γ_{Os}[b]	T_{RD} [Ga][c,d]	±[e]	T_{CHUR} [Ga][c,d]	±[e]
C1	0.145	0.039	0.1043	0.0088	1	−17.9	3.3	1.3	5.1	2.3
C3	0.064	0.042	0.1066	0.0057	1	−16.1	3.00	0.82	3.6	1.2
C4	0.272	0.017	0.1222	0.0048	1	−3.80	0.76	0.71	2.2	2.1
C19	0.566	0.036	0.1158	0.0024	1	−8.83	1.74	0.35	−4.23	0.31
C20	0.0604	0.0045	0.1103	0.0015	1	−13.2	2.47	0.22	2.88	0.28
C23	0.2102	0.0078	0.1200	0.0025	1	−5.52	1.07	0.37	2.17	0.76
C24	0.301	0.022	0.1208	0.0064	1	−4.92	0.97	0.96	3.6	3.6
C25	0.024	0.016	0.1064	0.0054	1	−16.2	3.01	0.77	3.19	0.91
C27	0.1287	0.0040	0.1651	0.0077	1	30.0	na	na	−9.0	1.8
C38	0.0134	0.0057	0.1083	0.0020	1	−14.8	2.75	0.29	2.84	0.33
C41	0.1118	0.0013	0.1002	0.0020	1	−21.1	3.90	0.29	5.33	0.39
C43	0.1426	0.0026	0.4732	0.0093	1	272	na	na	na	na
C78	0.010130	0.000026	0.10786	0.00026	1	−15.1	2.808	0.037	2.878	0.037
C79	0.0453	0.0068	0.1584	0.0015	1	24.7	na	na	−5.55	0.16
C80	0.03594	0.00016	0.11478	0.00022	1	−9.66	1.816	0.032	1.986	0.030
C158	0.0842	0.0010	0.11999	0.00094	1	−5.56	1.06	0.14	1.32	0.16
C185	0.006101	0.000056	0.10776	0.00042	1	−15.2	2.822	0.060	2.864	0.060
C186	0.385	0.010	0.1523	0.0034	1	19.9	na	na	na	na
C205	0.3931	0.0054	0.1525	0.0016	1	20.1	na	na	na	na
C206	0.09476	0.00064	0.11586	0.00044	1	−8.81	1.667	0.064	2.155	0.070
C211	0.01175	0.00022	0.1082	0.0014	1	−14.8	2.76	0.20	2.84	0.20
C216	2.713	0.056	0.2778	0.0048	1	119	na	na	3.79	0.14
C217	0.649	0.012	0.1644	0.0034	1	29.4	na	na	8.4	1.0
C231	0.1723	0.0010	0.12449	0.00024	1	−2.02	0.408	0.036	0.669	0.020
VR16367	0.0395	0.0094	0.1068	0.0024	2	−16.0	2.97	0.34	3.28	0.44
VR19674	0.0133	0.0015	0.1102	0.0020	2	−13.2	2.47	0.29	2.55	0.30
VR40383	0.0961	0.0050	0.11308	0.00076	2	−11.0	2.07	0.11	2.69	0.17
VR481	0.013719	0.000078	0.10797	0.00014	2	−15.0	2.793	0.020	2.888	0.019
VR50882	0.541	0.015	0.11135	0.00084	2	−12.4	2.38	0.12	−7.15	0.78
VR50904	0.18	0.10	0.1400	0.0090	2	10.2	na	na	−3.68	0.55
YK2471	0.401	0.017	0.1251	0.0062	1	−1.55	0.35	0.93	na	na

Uncertainties on isotope ratios are 2 standard errors. γ_{Os} calculated as the present-day percent deviation of the samples from chondritic mantle (values of Walker et al., 1994). T_{RD} are rhenium-depletion ages (Walker et al., 1989), T_{CHUR} are model ages, calculated for extraction from a chondritic (CHUR) source (values of Walker et al., 1994) and using a λ for ^{187}Re of 1.666×10^{-11} a^{-1} (Smoliar et al., 1996). Ages are given irrespective of plausibility or precision.

[a] (1) this study; (2) Pearson et al. (1999).

[b] Percent deviation from $^{187}Os/^{188}Os$ of chondrite today (values of Walker et al., 1994).

[c] Calculated assuming formation from a chondritic reservoir (Walker et al., 1994).

[d] Corrected for ingrowth of ^{187}Os since kimberlite-eruption ~ 60 Ma ago.

[e] Calculated using 2 Standard errors on $^{187}Os/^{118}Os$ or combining 2 Standard errors on $^{187}Re/^{188}Os$ and $^{187}Os/^{188}Os$.

of the mss have a geological origin, and do not represent contamination or an analytical artefact:

(1) No W-rich materials were used in the sample preparation; in particular no tungsten–carbide mills were used at any time; (2) high W contents were found using three different methods, i.e., EMP analysis (of the Fe metal), quadruple ICPMS and multicollector ICPMS; (3) W abundances were obtained by drilling into the sulfide (~ 0.7–1.2 μm/s, for 50- to 100-s runs), and W signals for the high-W materials were sustained well above background for >70 s (Fig. 7). Integration of the signal was done from about 10 s after the ablation started to exclude ablated material deposited at the surface and other surface contamination; (4) host olivine and sulfides from Lac de Gras were prepared in the same manner as a suite from Siberia, yet sulfides from Siberia have W contents < 40 ppm with the exception of one sulfide with 165 ppm (Griffin et al., 2002).

Tungsten appears to be homogeneously distributed in the W-rich sulfides and is not correlated with O-content (Fig. 6d). Therefore, the W-rich oxides in the Fe metal are considered to be exsolution products from a single W-bearing precursor metal phase similar to that reconstructed from Fe metal and W-rich oxides.

5. Re–Os isotope systematics

Re–Os isotope data for 24 Fe-rich mss inclusions in concentrate-derived minerals and for one included sulfide grain in a xenolith from Lac de Gras (this study) were combined with results for six Lac de Gras samples given by Pearson et al. (2002), of which one is an inclusion in diamond, one is an inclusion in an olivine macrocryst and four are from peridotites (Table 5). The data set in this study encompasses $^{187}Os/^{188}Os$ ratios from 0.1002 to 0.4732, corresponding to subchondritic γ_{Os} ($\gamma_{Os}=\{[(^{187}Os/^{188}Os_{sample})/(^{187}Os/^{188}Os_{chondrite})] - 1\} \times 100$) for all but eight samples. $^{187}Re/^{188}Os$ range from 0.006 to 2.713. Re–Os isotope systematics are shown in Fig. 8.

Re-depletion ages (T_{RD}, Walker et al., 1989) were calculated for samples with negative γ_{Os} (Table 5). They range from 0.35 to 3.9 Ga. Four samples have T_{RD}>3.0 Ga, six samples give ~ 2.75–2.97 Ga, and the remainder give younger ages. Model ages (T_{MA}) for eight samples are negative (future) or implausibly old, having either unsupported radiogenic Os (light grey field in Fig. 8) or low $^{187}Os/^{188}Os$ relative to their Re/Os, suggesting recent Re addition (stippled line in Fig. 8). Five samples give T_{MA}> 3.2 Ga, six

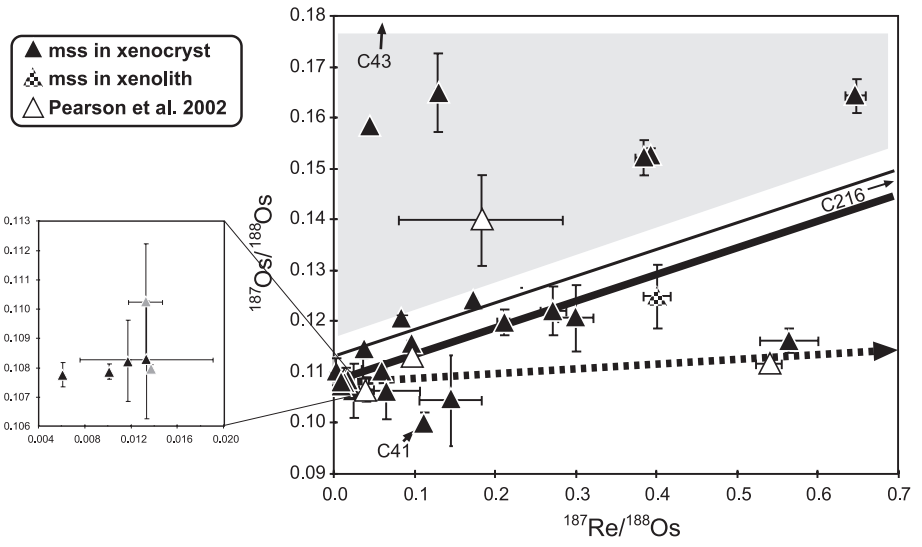

Fig. 8. Re–Os isotope diagram for concentrate- and xenolith-derived sulfides from this study and from Pearson et al. (2002). One area of the diagram has been blown up for resolution. Error bars are two standard errors (2 S.E.). Four different groups with respect to Re–Os isotope systematics are indicated by three trends (solid and stippled lines) and the grey field will be discussed in the text. The sulfide with the most unradiogenic Os (C41) is also indicated.

samples give 2.8–2.9 Ga and the remainder give younger ages, down to 0.7 Ga (Table 5).

Richardson et al. (2001) report up to 30% relative difference in $^{187}Re/^{188}Os$ for different fragments of low-temperature assemblages of pyrrhotite, pentlandite and chalcopyrite included in eclogitic diamonds, which they ascribe to partitioning of Re into the chalcopyrite and incomplete recovery of the inclusion during sample preparation. It is possible that during the in situ isotope analysis, the sulfides were not sampled in modal proportions, as already discussed for the trace-element data. In this study, Re–Os data were collected by focussing the laser beam on the centre of the sulfides and in the majority of the analyses, the sulfide was totally consumed. However, it is possible that chalcopyrite, which occurs mostly on the rims, is not adequately represented, leading to spuriously low $^{187}Re/^{188}Os$ in some samples. This could lead to T_{CHUR} overestimates for samples with supra-chondritic γ_{Os}, and underestimates for those with subchondritic γ_{Os}. In contrast, the effect on $^{187}Os/^{188}Os$ would be negligible because the exsolution into low-temperature assemblages including chalcopyrite occurred relatively recently (ca 50 Ma), during eruption of the kimberlite (Richardson et al., 2001). In most cases, because the sulfide grain was consumed during Re–Os analysis, no modal bias on Re–Os ages is expected.

6. Host compositions

Three of the sulfide inclusions are hosted by orthopyroxene, one is hosted by clinopyroxene, two sulfide grains were recovered without a host and the rest are included in olivine. Mss occur in olivine with Mg-numbers (Mg# = 100Mg/(Mg + Fe)) ranging from 88.6 to 93.7 (mean = 91.7), whereas $(Ni,Co,Fe)_{3-x}S_2$ are hosted by olivine with Mg# from 87.2 to 92.0 (mean = 90.4) (Table 6). Many host silicates have Mg#, CaO and NiO contents similar to olivine from Lac de Gras peridotite xenoliths (Pearson et al., 1999; authors' unpublished data). The compositional overlap suggests that the xenocrystic hosts originated by disaggregation of lithospheric mantle material. This interpretation is supported by the occurrence of both included and interstitial sulfides, including $(Ni,Co,Fe)_{3-x}S_2$, in peridotitic xenoliths from Lac de Gras (Pearson et al., 1999; authors' unpublished data). The compositions of sulfide-hosting olivine trend towards lower Mg# and both unusually high and low NiO contents relative to olivine from xenoliths and diamonds. The low Ni contents suggest melting at high pressures, as olivine-melt partition coefficients decrease with increasing pressure, from 3.0 at 1 GPa to 1.4 at 14 GPa (Bickle et al., 1977; Suzuki and Akaogi, 1995).

There is no correlation between NiS (Ni/(Ni + Fe)) of sulfide and NiO of coexisting olivine. Mss–olivine pairs have K_Ds for the exchange of Ni and Fe between olivine and sulfide that are lower (0.2–27) than the equilibrium high-temperature K_D of 32 adopted by Fleet and Stone (1990) and most are lower than the range of K_Ds of 17–56 in high-temperature, ambient-pressure experiments of Gaetani and Grove (1997). In contrast, K_Ds for $(Ni,Co,Fe)_{3-x}S_2$-olivine pairs trend towards much higher values (51–272).

The Ca-in-olivine thermometer (Köhler and Brey, 1990) was applied under the assumption that the olivine xenocrysts were in equilibrium with clinopyroxene. This is supported by the Ca-saturation of

Table 6
Average composition of host minerals in wt.%

Mineral	*n*	SiO_2	FeO^t	MnO	MgO	CaO	NiO	Total	Mg#	Ca[a]	$T_{Ca\text{-in-ol}}$[b]
Avg ol hosting mss	42	40.85	8.16	0.11	50.52	0.04	0.36	100.2	91.7	321	1186
Avg ol hosting $(Ni,Co,Fe)_{3-x}S_2$	10	41.52	9.32	0.12	49.09	0.04	0.35	100.5	90.4	353	1202
ol hosting Fe metal	1	40.97	8.44	0.10	49.58	0.26	0.22	100.0	91.3	240	1151
Avg opx hosting mss	3	58.13	5.12	0.10	35.37	0.59	0.09	100.5	92.5		
cpx hosting $(Ni,Co,Fe)_{3-x}S_2$	1	55.14	3.56	0.09	17.97	18.15	< 0.08	99.3	90.0		

Temperatures, calculated using the Ca-in-olivine thermometer of Köhler and Brey (1990) at a nominal pressure of 5 GPa, require cpx to be part of the assemblage and the average composition of clinopyroxene in xenoliths from Lac de Gras (Pearson et al., 1999, and unpublished data) was used for the temperature calculation. Abbreviations as in Table 2.

[a] (ppm).

[b] (°C).

garnets in 59 out of 63 xenoliths from Lac de Gras (Pearson et al., 1999; authors' unpublished data). At a nominal pressure of 2 GPa, temperatures range from 960 to 1090 °C, and at 5 GPa, temperatures range from 1100 to 1300 °C. This places the host olivine in the deep lithospheric mantle stratum, which extends from ca. 140- to 220-km depth (Griffin et al., 1999; although 2 GPa is lower than pressures expected in the deep lithospheric mantle layer, temperatures were calculated for this pressure to ensure that temperatures expected in the deep layer were obtained regardless of the choice of pressure).

7. Discussion

7.1. Inclusion–host relationships

The wide range of K_Ds for the distribution of Ni and Fe between olivine and included sulfides suggests that different inclusion–olivine pairs attained variable degrees of equilibrium during or after transport in the host kimberlite to lower temperatures than indicated by the Ca-in-olivine temperatures. Since we are dealing with isolated olivine xenocrysts instead of an infinite olivine reservoir, the effect of reequilibration was probably more pronounced in the single olivine, where the abundances of Ni and Fe are low compared to sulfide. The contrast between mss-olivine K_Ds and $(Ni,Co,Fe)_{3-x}S_2$-olivine K_Ds may indicate that bulk composition has an effect on the distribution of Fe, Co and Ni between these phases.

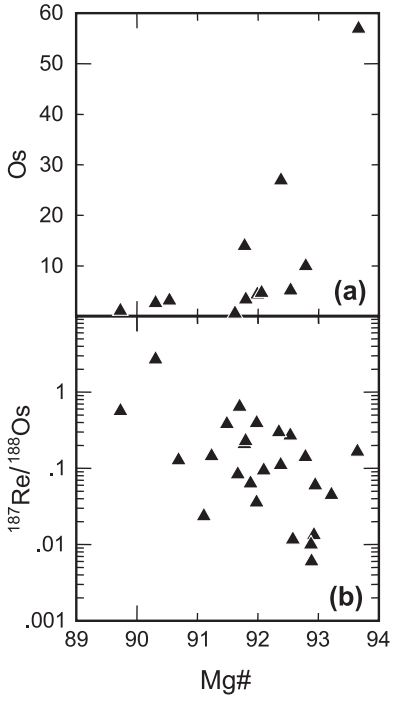

Fig. 9. Mg-number in olivine versus (a) Os (in ppm) and (b) $^{187}Re/^{188}Os$ in mss.

The weak covariations of Os abundance and $^{187}Re/^{188}Os$ in sulfide with Mg# in olivine (Fig. 9) suggest that the relationship between these two phases is not accidental. It could be interpreted in terms of a co-evolution of metasomatic sulfide and silicate melts and their interaction with peridotite, but would also be qualitatively consistent with magmatic fractionation in both the silicate and sulfide portions of the source.

7.2. Open-system behaviour

Os and Ir are well correlated in mss from Lac de Gras (Fig. 10a). Ir also correlates positively with Ru and Rh and demonstrates the geochemical affinity of these elements. These covariations may reflect a primary igneous trend, where early crystallising sulfide has high concentrations, whereas the fractionated sulfide melt has low concentrations. Alternatively, Os and Ir are partitioned into a residual sulfide, whereas the complementary sulfide melt has low concentrations. While a crude positive correlation is recognisable for incompatible elements (Pd, Pt), the scatter is larger than for compatible elements (Fig. 10b).

Some of the scatter in the incompatible PGE could be due to secondary processes, such as interaction with melts and fluids. The variable trace-element abundances may also reflect a combination of sulfide liquid trapped with the sulfide and variable formation conditions, as the partitioning of PGE between sulfide and sulfide melt depends on bulk composition of the system, pressure, temperature, and partial pressures of oxygen and sulfur (see review by Makovicky, 2002). The negative Pt anomalies (Fig. 5a,b,d) could be explained by the presence of pre-existing or exsolved alloys (e.g., Orberger et al., 1998) that were not trapped with the sulfides. Pt may also have been removed from sulfide in sulfurous vapours together with Cu and Ni (Baker et al., 2001).

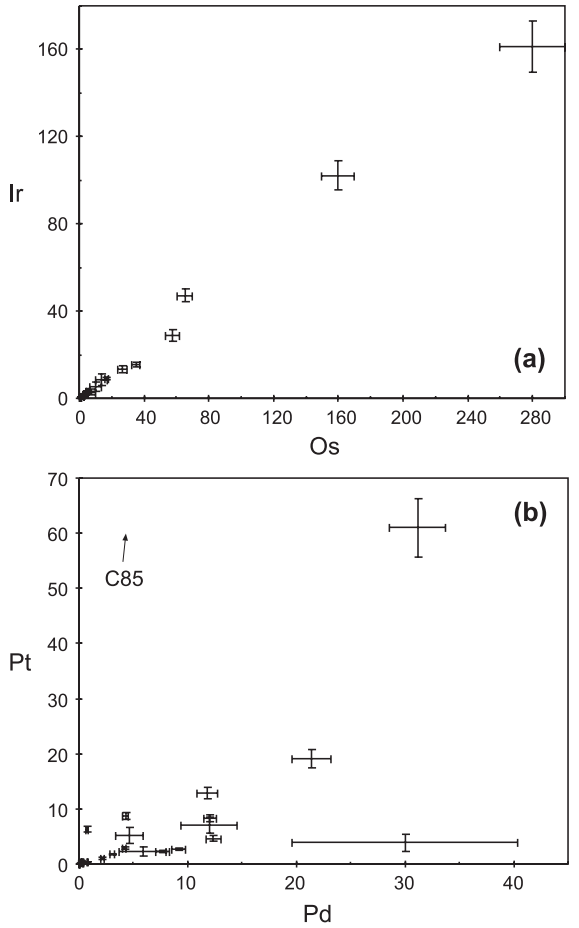

Fig. 10. Diagram of (a) Os versus Ir and (b) Pd versus Pt in mss. Error bars are 1σ (within-run precision) or 1 standard deviation (external precision), whichever is higher. Abundances in ppm.

The high-W sulfides tend to have higher As contents, though W and As are uncorrelated. Other samples display relatively high Zn contents, a feature also seen in some sulfide inclusions in olivine from Siberia (Griffin et al., 2002). Arsenic and Zn are soluble in moderately saline, high-H_2S fluids, whereas W and Mo favour saline H_2S-deficient fluids in hydrothermal systems (Noll et al., 1996). The enrichment in W, As and Zn and the fact the these elements do not behave sympathetically suggests repeated interaction with fluids of different composition. Interaction with fluids could explain the disturbed incompatible PGE budget and implausible model ages in samples with unsupported radiogenic Os or recent Re-enrichment. The sulfides may have been trapped in the host silicates during metasomatism, possibly upon mantle recrystallisation (Drury and Van Roermund, 1989) induced by the fluid percolation.

7.3. Possible origins of mss, $(Ni,Co,Fe)_{3-x}S_2$ and Fe metal

7.3.1. Primary mss, secondary $(Ni,Co,Fe)_{3-x}S_2$ and Fe metal

Mss in olivine xenocrysts from Lac de Gras may be interpreted as part of a residual mantle assemblage after partial melting (e.g., Lorand, 1987). A test as to which of the samples represent undisturbed products of high-temperature fractionation is to compare their trace-element compositions to those produced by melting of hypothetical primitive sulfide, which has been calculated following Peach et al. (1990; Table 7). Fig. 11 shows the position of all samples in the Pt–Ir–Pd ternary diagram relative to an estimated igneous trend, defined by compositions of sulfide melts and complementary residues that were calculated for the partitioning of these elements between mss and

Table 7
Trace-element modelling

	Pt	Ir	Pd
Primitive mantle	0.0071	0.0032	0.0039
Primitive sulfide	9.372	4.224	5.148
S-Saturated system			
$D_{mss/sulf\ liquid}$	0.1	4.0	0.1
10% batch melt	64.6	1.1	27.1
40% batch melt	21.8	1.5	11.2
80% batch melt	11.6	2.6	6.3
0.5% fract. melt	170.4	1.1	49.2
1% fract. melt	154.9	1.1	47.0
10% fract. melt	25.3	1.1	19.9
Residue 10% batch	3.2	4.6	2.7
Residue 40% batch	1.1	6.0	1.1
Residue 80% batch	0.6	10.6	0.6
Residue 0.5% fract.	8.5	4.2	4.9
Residue 1% fract.	7.7	4.3	4.7
Residue 10% fract.	1.3	4.6	2.0

Primitive sulfide with 33 wt.% sulfur (=average for sulfides from Lac de Gras) was calculated from primitive mantle values of McDonough and Sun, (1995). Experimental distribution coefficients for the partitioning of PGE between mss and sulfide liquid $D_{mss/sulf\ liquid}$ (Li et al., 1996; experiments at 1100 °C and 35 wt.% S content) were used to calculate partial melts and complementary residues assuming batch and fractional melting models.

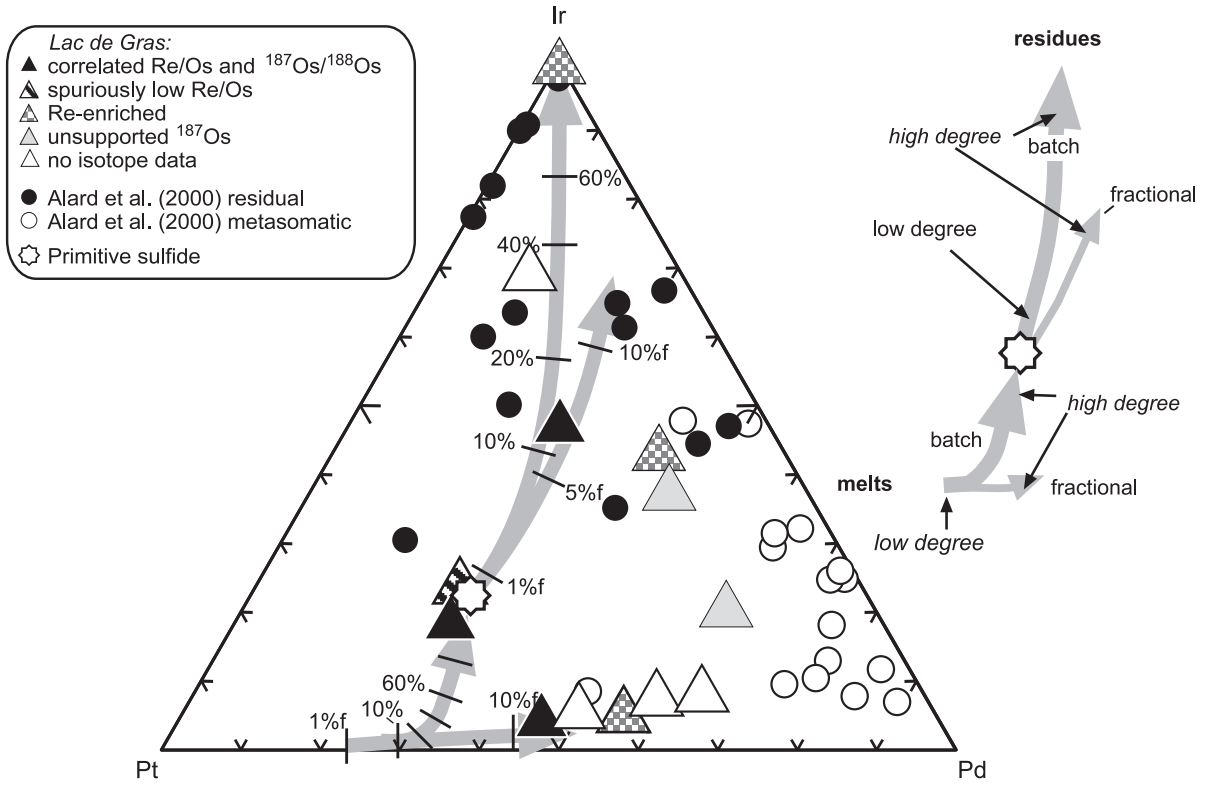

Fig. 11. Tri-plot of the Platinum-group elements Pd, Ir and Pt in mss against a calculated igneous trend (grey arrows) defined by partial melts and residues of a primitive mantle sulfide (Table 7). Inset shows the trends for different melting models (batch and fractional melting). Arrows indicate increasing degrees of partial melting. Different groups of samples with regard to Re–Os isotope systematics are indicated (see section 7.4.1). Metasomatic (i.e., interstitial) and residual (i.e., enclosed) sulfides of Alard et al. (2000) are shown for comparison.

sulfide melt using values of Li et al. (1996). While some samples plot on or close to the igneous trend, many samples lie to the Pd-rich or Pt-depleted side, suggesting the operation of secondary processes.

Before we discuss the possible origins of (Ni,Co,Fe)$_{3-x}$S$_2$, we would like to emphasise that this phase occurs also as an inclusion in diamond from Lac de Gras (Davies et al., in prep). Therefore, deuteric alteration processes or loss of sulfur and Fe en route to the surface, due to the fracturing of host olivine grains during decompression (Lorand, 1990), are unlikely to be the reasons for the unusual composition of (Ni,Co,Fe)$_{3-x}$S$_2$. However, this does not preclude that such processes also occurred.

A few low-temperature assemblages similar to those from which the (Ni,Co,Fe)$_{3-x}$S$_2$ was reconstructed have been observed in alpine mantle peridotites and in mantle xenoliths from central Europe; they were ascribed to low-temperature fluid-related processes involving the replacement of pentlandite by heazlewoodite and magnetite (Garuti et al., 1984; Szabó and Bodnar, 1995). Oxygen contents in (Ni,Co,Fe)$_{3-x}$S$_2$ are no higher than in mss, and a ferric-iron rich phase has only been observed in the low-temperature assemblage of one grain. The involvement of oxidising fluids in the formation of (Ni,Co,Fe)$_{3-x}$S$_2$ is therefore unlikely. By contrast, reducing fluids may have led to desulfidisation (e.g., Lorand and Conquéré, 1983) and formation of Fe metal by exsolution from olivine or from mss, leaving behind S- and Fe-poor (Ni,Co,Fe)$_{3-x}$S$_2$. If (Ni,Co,Fe)$_{3-x}$S$_2$ originated by alteration of primitive sulfides in the deep lithosphere (the depth being constrained by its inclusion in diamond), it is surprising that more of these sulfides or their low-temperature products have not been observed (Figs. 3 and 4).

7.3.2. Igneous origin of mss and $(Ni,Co,Fe)_{3-x}S_2$

The fact that $(Ni,Co,Fe)_{3-x}S_2$ and mss from Lac de Gras form compositionally distinct clusters similar to $(Ni,Fe)_{3\pm x}S_2$ in equilibrium with mss and residual liquid in the Fe–Ni–S system (Karup-Møller and Makovicky, 1995; Fig. 3) would be consistent with an igneous origin for both sulfide types. The phase diagram shows that a Ni-rich sulfide melt could first precipitate Ni-rich mss, followed by precipitation of $(Ni,Co,Fe)_{3-x}S_2$ in equilibrium with a residual Cu-rich melt. Tie-lines connecting experimental $(Ni,Fe)_{3\pm X}S_2$ and mss are steeper than a hypothetical tie-line connecting average $(Ni,Co,Fe)_{3-x}S_2$ and mss from Lac de Gras. Also, experimental $(Ni,Fe)_{3\pm x}S_2$ appears at a lower temperature than those obtained from olivine hosting $(Ni,Co,Fe)_{3-x}S_2$. This may indicate that $(Ni,Co,Fe)_{3-x}S_2$ formed by a similar mechanism but under different conditions, e.g., higher *P*/*T*. However, primitive mantle is not expected to produce such Ni-rich melts. This leads to the more speculative part of the model.

During core formation, carbon-bearing metal-rich sulfide melts drained to the core and some of this metal may have been trapped in the mantle (Rama Murthy and Hall, 1972; Arculus and Delano, 1981). Such melts would form two immiscible melts upon cooling: a S-, Ni- and Co-poor metal melt, and a Ni- and Co-rich sulfide melt (Ballhaus and Ellis, 1996; Jana and Walker, 1997). Ni-rich mss, such as that observed in xenocrystic olivine from Lac de Gras, would precipitate from the S-rich melt, but at Fe/Ni and Fe/Co>1. The fractionated melt would be depleted in S and enriched in Ni and Co, and precipitate $(Ni,Co,Fe)_{3-x}S_2$, which has lower Me/S. Liquid immiscibility could be induced during ascent of a plume from the deep mantle that entrained lower mantle material including the trapped metal component. Assuming that the phase changes during ascent into the upper mantle are isochemical, the two sulfide types could be trapped by recrystallising olivine. Intriguingly, the Fe metal has marked negative Ni and Co anomalies that might be expected in the unmixed S-, Ni- and Co-poor metal melt.

7.4. Interpretation of Re–Os isotope systematics

7.4.1. Comparison of Os isotope composition and HSE abundances

In the Re–Os isotope diagram (Fig. 8), five groups of sulfides have been distinguished: sulfides with unsupported $^{187}Os/^{188}Os$, sulfides that have correlated $^{187}Os/^{188}Os$ and $^{187}Re/^{188}Os$, sulfides with spuriously low Re/Os, sulfides lying on a trend of recent Re-enrichment and one sulfide with significantly lower $^{187}Os/^{188}Os$ than those lying on the correlation or the Re-enrichment trend. In the following, we will eval-

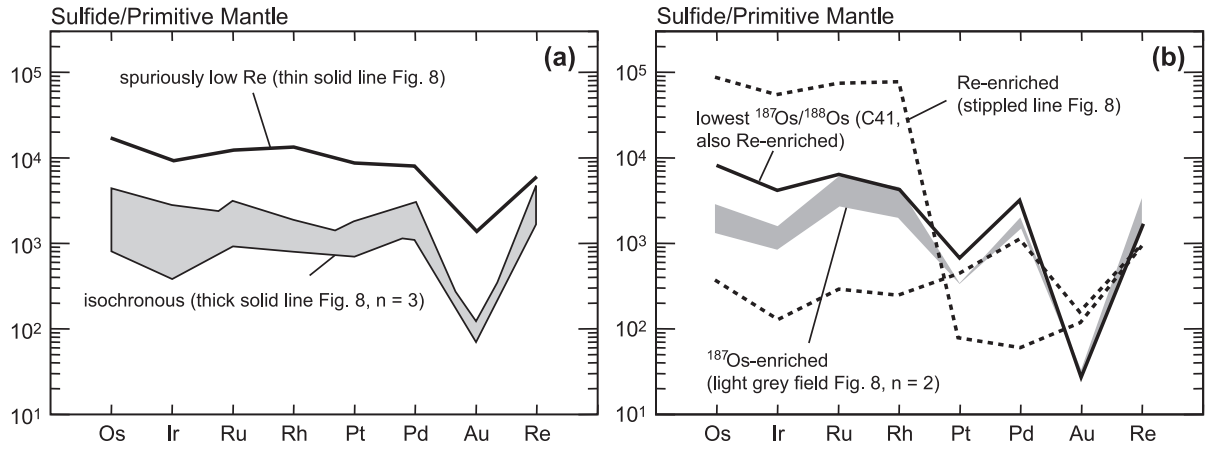

Fig. 12. Extended PGE-patterns normalised to primitive mantle of McDonough and Sun (1995). Samples are grouped according to whether they (a) lie on the 11-point isochron, have assumed undersampled Re, or (b) are ^{187}Os- or Re-enriched. Location of samples with regard to the trends and fields in the Re–Os isotope diagram (Fig. 8) is also indicated.

uate if disturbances in the Re and/or Os budget will produce distinct signatures in the other HSE. Note, however, that HSE data are not available for many of the sulfides due to complete consumption during Re–Os isotope analysis, which was carried out prior to trace-element analysis.

Trace-element data are available for three of the samples having correlated $^{187}Os/^{188}Os$ and $^{187}Re/^{188}Os$ (including high-Re/Os sample C216) and they plot on the igneous trend in Fig. 11. Their extended PGE patterns are relatively flat, with the exception of Au (Fig. 12a).

One sulfide with spuriously low Re/Os, due to insufficient sampling of exsolved Re-rich cp rims during laser ablation, also plots on the igneous trend in Fig. 11. This may indicate that the PGE do not follow Re upon low-temperature re-equilibration and exsolution of cp. With the exception of Au, the extended PGE pattern is similar to those of sulfides lying on the main trend, though displaced to higher abundances (Fig. 12a).

Some sulfides have highly radiogenic Os isotopic compositions that are not supported by their Re/Os; their $^{187}Re/^{188}Os$ is too low to have produced the observed radiogenic Os within the age of the solar system. HSE data were obtained for two of these sulfides and they plot to the Pd/Pt-rich and Pd/Ir-rich side in Fig. 11, away from the igneous trend, and towards the interstitial metasomatic sulfides of Alard et al. (2000). Also, their primitive mantle-normalised (indicated by the suffix$_{PM}$) extended PGE-patterns (Fig. 12b) show the highest Ru/Os and Ru/Ir of all samples.

Sulfides with low $^{187}Os/^{188}Os$ relative to their Re/Os (Re-enriched samples) appear to lie on a sub-horizontal trend which originates within error at the initial $^{187}Os/^{188}Os$ of the samples with correlated $^{187}Os/^{188}Os$ and $^{187}Re/^{188}Os$ (Fig. 8). This trend is interpreted as reflecting Re-enrichment. One of two samples plots on the Pd-rich side in the Pt–Ir–Pd ternary plot (Fig. 11). The other sample plots at the Ir-apex. Their undisturbed Os isotope composition suggests that the Re enrichment did not entail a modification of the compatible PGE budget and their extended PGE_{PM} patterns give no definite indication that any disturbance has occurred (Fig. 12b).

Sulfide C41 has significantly lower $^{187}Os/^{188}Os$ than other sulfides from Lac de Gras and also appears to have suffered mild Re-addition, given its 5.1 Ga model age. It has an extremely low Au abundance, but its extended PGE_{PM} pattern does not portray its Re enrichment nor its extremely low $^{187}Os/^{188}Os$.

7.4.2. Model ages

Model ages (T_{CHUR} and T_{RD}; rhenium-depletion age as defined in (Walker et al., 1989) have been

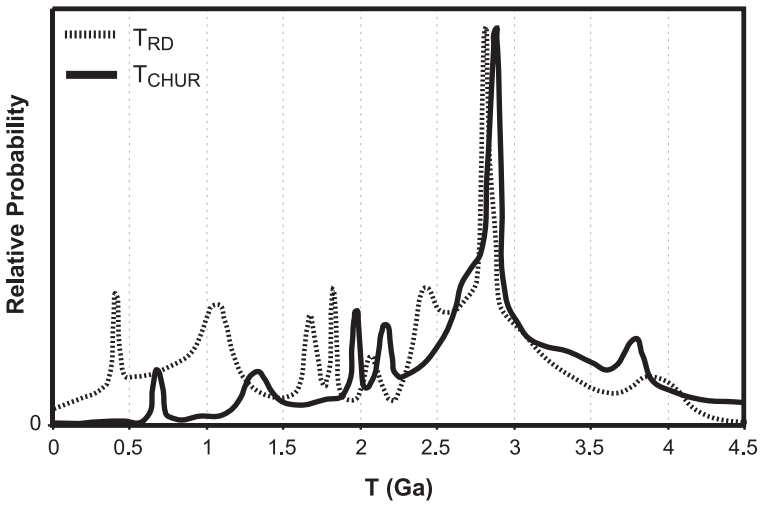

Fig. 13. Cumulative probability diagram (using Isoplot of Ludwig, 1999) of rhenium-depletion ages (T_{RD}, as defined by Walker et al., 1989) and model ages (T_{CHUR}, as given in Table 5; model parameters of Walker et al., 1994).

calculated by reference to the mantle evolution curve of Walker et al. (1994). This particular curve has been chosen to facilitate comparison and is not meant to have any genetic significance. Because all of the host olivines were entrained from the deep lithospheric mantle layer, the age data pertain to that mantle stratum only. In a cumulative probability plot, several modes are evident, both for T_{RD} ages and T_{CHUR} ages (Fig. 13). A strong peak is apparent at ca. 2.8 Ga for T_{RD} and 2.9 Ga for T_{CHUR}. These ages exceed that of the overlying crust, the 2.7 Ga turbidites of the Contwoyto terrane. Some peaks at younger ages could be correlated with events in the Slave Craton, such as the Malley-McKay (2.2 Ga) and Mackenzie dike swarms (1.27 Ga), suggesting crystallisation of sulfides from asthenosphere-derived melts (Griffin et al., 2003(a)). However, these peaks may also reflect mixing of older and younger components and may not carry any real age information. Sample C41 has extremely unradiogenic $^{187}Os/^{188}Os$ and gives a T_{RD} of 3.9 ± 0.29 Ga.

7.4.3. Isochron

An isochron constructed from 11 samples (Fig. 14) yields an initial $^{187}Os/^{188}Os$ of 0.10725 ± 0.00014 (γ_{Os} = 2.53 ± 0.13) at 3.27 ± 0.34 Ga (MSWD = 0.75).

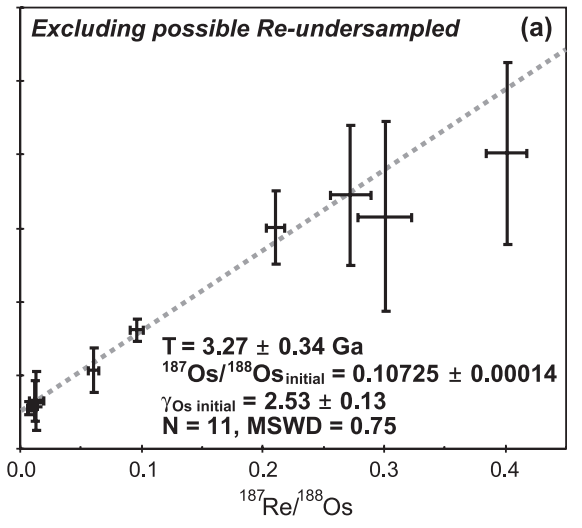

Fig. 14. Isochron (model 1 solution; using Isoplot of Ludwig, 1999) constructed with 11 samples. Error bars are 2 S.E. Samples used are: C4, C20, C23, C24, C38, C78, C185, C211, YK2471, VR481, VR40383.

The initial Os isotope composition is enriched relative to chondritic mantle. These samples were chosen primarily because they lie on a trend that includes the high-Re/Os sample C216. Sample C216 was not used in the regression because we cannot confidently correct for large overlaps of ^{187}Re on ^{187}Os. The range in Re/Os among these samples is interpreted as the product of magmatic fractionation, where C216 represents a trapped sulfide liquid, while low-Re/Os samples represent residual mss and intermediate-Re/Os samples represent mildly depleted mss or a mixture of residual mss and trapped sulfide liquid. Trace-element abundances are available for three of the isochronous samples and all three lie on the calculated igneous trend in Fig. 11. By contrast, five of six samples with unsupported radiogenic ^{187}Os and assumed Re-enriched samples plot off the calculated igneous trend.

The positive γ_{Os} of 2.53 ± 0.13 for the sulfide suite is identical to that estimated for the outer core at 3.27 Ga (parameters of Walker et al., 1995), suggesting that transfer of outer core material into the mantle or isotopic equilibration with the outer core could be at the origin of the high initial $^{187}Os/^{188}Os$ (Walker et al., 1995, 1997; Brandon et al., 1998; Puchtel and Humayun, 2000). Alternatively, the lower mantle may have supra-chondritic Re/Os because more Os than Re partitioned into the core relative to the silicate portion (Walker et al., 1997). Mixing of this Re-enriched lower mantle (parameters of Walker et al., 1997) with 23% chondritic mantle would satisfy the requirements of the isochron. Finally, a deep mantle source may have been enriched by recycling of ~ 30% of ~ 260 Ma old (at 3.27 Ga) basaltic crust to chondritic mantle, which would raise the $^{187}Os/^{188}Os$ of the source to the required value.

The Os isotope evolution trajectory of a modelled high-Re/Os lower mantle source passes through the initial γ_{Os} of lithospheric mantle samples and mantle-derived melts from 3.8 Ga ago to the present and includes isochronous sulfides from Lac de Gras (Fig. 15). We take this to indicate that our regression and the result are meaningful and reasonable. On the other hand, this suggests that the lower mantle represents a long-lived ^{187}Os-enriched mantle domain that has been repeatedly tapped by plumes and upwelling mantle at least since the Meso-Archaean. A second group of samples plot along the chondritic evolution line (Fig. 15), suggesting that it, too, has been an

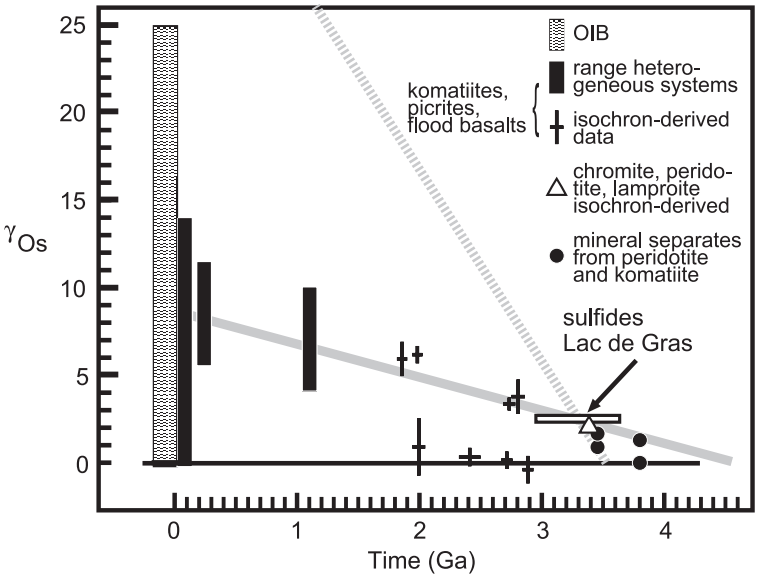

Fig. 15. Diagram of time versus γ_{Os} (after Walker and Nisbet, 2002), for sulfides from Lac de Gras (isochron-derived), chromite, lherzolite and lamproite from the 3.4 Ga Kimberley block (Western Australia; isochron-derived; Graham et al., 1999), olivine and spinel separates from 3.8 Ga West Greenland spinel peridotites and chromite separates from 3.46 Ga Pilbara komatiite (Bennett et al., 2002), and plume-derived melts (komatiites, picrites, flood basalts, OIBs) from 2.8 Ga through recent (from Walker and Nisbet, 2002, and references therein). Grey lines show γ_{Os} evolution for chondritic mantle enriched by addition of oceanic crust at 3.53 Ga and evolving at a $^{187}Re/^{188}Os$ of 1 (stippled line), and for lower mantle that was Re-enriched during core fractionation or interaction with the Re-enriched outer core at 4.55 Ga and evolving at $^{187}Re/^{188}Os$ of 0.54 (solid line). The black line shows the γ_{Os} evolution of chondritic mantle, which, by definition (Walker et al., 1989), has zero slope.

important long-lived reservoir, perhaps restricted to shallower mantle regions (cf. Bennett et al., 2002).

7.5. Implications for lithosphere formation

Model ages and the isochron age indicate that there is a component in the deep lithospheric mantle beneath the Contwoyto terrane that is significantly older than the overlying 2.7 Ga crust. Nd isotope data indicate formation of the crust from juvenile sources and the absence of older crust at depth (Davis and Hegner, 1992). If indeed the Re/Os data reflect 3.3 Ga melting of a radiogenic source, it coincides within error with a period of extensive crust formation in the adjoining Central Slave Basement Complex (CSBC; Bleeker et al., 1999), a 4.0–2.7 Ga continental block that collided with the Contwoyto terrane at 2.7 Ga. The isochron age is also consistent within error with lower crustal and mantle ages in other parts of the Contwoyto terrane (Grutter et al., 2000; Irvine et al., 2003). The old ages for lower crust and mantle samples in the Contwoyto terrane, combined with evidence that east-dipping subduction took place when the Contwoyto terrane and the CSBC collided (Bleeker et al., 1999), suggest the presence of a translithospheric discontinuity dating back to the assembly of the Slave Craton. This is consistent with the fact that the Lac de Gras kimberlites sit atop the Nd isotope line, which maps the terrane boundary at depth (Davis and Hegner, 1992; Davis, personal communication, 2003), and atop a strong gradient in lithospheric strength (Poudjom Djomani et al., 2003).

If the sulfide-derived isochron carries real age information, there are a number of features that are consistent with a plume origin for the deep lithosphere, as originally proposed by Griffin et al. (1999). These are: the geochronological coincidence of voluminous crust formation and sulfide ages in the deep lithosphere, the supra-chondritic initial Os isotopic composition, the presence of diamonds with lower mantle inclusions (Davies et al., 1999) and the heterogeneity of the shallow mantle but relative homogeneity of the deep mantle across the Slave Craton (Griffin et al., in press). A lower mantle origin for the

deep lithosphere could also explain the presence of unusual Ni and Co rich sulfides, by fractionation from immiscible carbon-bearing metal-rich sulfide melts, as discussed above.

The high initial $^{187}Os/^{188}Os$ combined with the presence of a sulfide with extremely unradiogenic Os would also imply that lithospheric mantle may form from sources with non-chondritic and heterogeneous Os isotopic compositions. The argument for a plume source containing depleted oceanic mantle domains is strengthened by recent evidence for recycled Archaean oceanic lithosphere sampled by a modern plume (Schaefer et al., 2002). Interestingly, a suite of sulfide inclusions in diamonds from the Panda pipe (adjacent to Lac de Gras) forms an isochron at 3.4 ± 0.28 Ga with a high initial $^{187}Os/^{188}Os$ of 0.10928 ± 0.00013 (Westerlund et al., 2003). While the age coincides within error with our results, the initial $^{187}Os/^{188}Os$ is significantly higher and could be interpreted as further evidence for heterogeneities in the plume. The possibility of subcretion of heterogeneous mantle as a mode of lithosphere formation in the Archaean suggests that model ages (T_{CHUR} or T_{RD}) may be inaccurate even for residual mantle peridotites, if the initial Os isotopic composition is not constrained.

8. Conclusions

We have analysed a suite of sulfide inclusions and one grain of Fe metal in xenocrystic olivine and pyroxenes from kimberlites in the Lac de Gras area, Slave Craton. The sulfide suite comprises unusual W-enriched sulfides with the non-stoichiometric composition $(Ni,Co,Fe)_{3-x}S_2$, and W-enriched mss. Based on the similarity of host silicates to peridotite minerals and the occurrence of similar sulfide inclusions in peridotites from the same locality, the samples are interpreted as disaggregated mantle material. Host olivines give temperatures (Köhler and Brey, 1990) that place the samples in the deep layer of the stratified lithospheric mantle beneath Lac de Gras (Griffin et al., 1999) and their chemical and isotopic composition may have a bearing on the formation and evolution of this layer.

Weak covariations between Os abundance and Re/Os of mss and the Mg# of host olivine would be compatible with a magmatic origin that was later obscured by repeated interaction with fluids, leading to unrelated W, As and Zn enrichments. $(Ni,Co,Fe)_{3-x}S_2$ could be interpreted as desulfidisation products, resulting from loss of S and Fe from primary mantle sulfides. They would also be consistent with an igneous origin, where, following the fractionation of Ni-rich mss, they precipitate from Ni-rich sulfide melts. Such melts may unmix from carbon-bearing metal-rich sulfide melts expected in the lower mantle (Rama Murthy and Hall, 1972; Arculus and Delano, 1981; Ballhaus and Ellis, 1996; Jana and Walker, 1997).

Mss give T_{RD} and T_{CHUR} ages with modes at 2.8 and 2.9 Ga, respectively, and extending to 3.9 Ga. Therefore, significantly older mantle resides beneath the western part of the 2.7 Contowyto terrane, where the Lac de Gras kimberlites intruded. This age paradox may be reconciled by thrusting of ancient mantle from the neighbouring 4.0–2.7 Ga CSBC beneath the Contwoyto terrane during 2.7 Ga collision (Bleeker et al., 1999). A subset of samples lies on a 3.27 ± 0.34 Ga isochron with supra-chondritic initial Os isotopic composition. If the isochron is real, the initial $^{187}Os/^{187}Os$ may be interpreted as the signature of a high-Re/Os source, such as the lower mantle or outer core which are thought to have evolved at supra-chondritic Re/Os (Walker et al., 1997). This would be consistent with an ultra-deep origin for the sulfides and the deep lithosphere in which they occur, in line with other lines of evidence that the deep lithospheric mantle beneath Lac de Gras is plume-derived (Griffin et al., 1999, in press(b); Davies et al., 1999). The presence of recycled oceanic mantle in the plume source is suggested by the presence of a sample with extremely unradiogenic $^{187}Re/^{187}Os$, pointing to heterogeneity in the plume source.

Acknowledgements

We are grateful to S. Graham for discussions and an informal review of the manuscript. C. Ballhaus, H. St. O'Neill and A. Woodland are thanked for the discussion and comments. An earlier version of this paper benefited from reviews by H. Becker, R. Carlson, D.G. Pearson and L. Reisberg. The current version was significantly

improved by the detailed reviews of C. Ballhaus, S.-J. Barnes, R. Carlson, B. Schaefer, C. Szabó and an anonymous reviewer, and by editorial comments by J.-P. Lorand and L. Reisberg. Help with the analytical facilities by S. Elhlou, C. Lawson and A. Sharma is gratefully acknowledged. This work was funded by a Macquarie University International Postgraduate Award and Postgraduate Research Fund (S.A.), by an ARC SPIRT grant sponsored by Kennecott Canada Inc., and by an ARC Large Grant to WLG and SYO'R. This is publication number no. 352 from the ARC National Key Centre for Geochemical Evolution and Metallogeny of Continents (www.es.mq.edu.au/GEMOC/). **[RR]**

References

Alard, O., Griffin, W.L., Lorand, J.P., Jackson, S.E., O'Reilly, S.Y., 2000. Non-chondritic distribution of the highly siderophile elements in mantle sulfides. Nature 407, 891–894.

Arculus, R.J., Delano, J.W., 1981. Siderophile element abundances in the upper mantle: evidence for a sulfide signature and equilibrium with the core. Geochim. Cosmochim. Acta 45, 1331–1343.

Baker, D.R., Barnes, S.-J., Simon, G., Bernier, F., 2001. Fluid transport of sulfur and metals between sulfide melt and basaltic melt. Can. Mineral. 39, 537–546.

Ballhaus, C., Ellis, D.J., 1996. Mobility of core melts during Earth's accretion. Earth Planet. Sci. Lett. 143, 137–145.

Bennett, V.C., Nutman, A.P., Esat, T.M., 2002. Constraints on mantle evolution from $^{187}Os/^{188}Os$ isotopic compositions of Archean ultramafic rocks from Southern West Greenland (3.8 Ga) and Western Australia (3.46 Ga). Geochim. Cosmochim. Acta 66, 2615–2630.

Bickle, M.J., Ford, C.E., Nisbet, E.G., 1977. The petrogenesis of peridotitic komatiites: evidence from high-pressure melting experiments. Earth Planet. Sci. Lett. 37, 97–106.

Bleeker, W., Ketchum, J.W.F., Jackson, V.A., Villeneuve, M., 1999. The Central Slave Basement Complex. Part I: its structural topology and autochthonous core. Can. J. Earth Sci. 36, 1083–1109.

Brandon, A.D., Walker, R.J., Morgan, J.W., Norman, M.D., Prichard, H.M., 1998. Coupled ^{186}Os and ^{187}Os evidence for core–mantle interaction. Science 280, 1570–1573.

Bulanova, G.P., Zayakina, N.V., 1991. Graphite–iron–cohenite assemblage in the central zone of diamond from 23rd party congress kimberlite. Dokl. Akad. Nauk SSSR 317, 706–709 (in Russian).

Cabri, L., 1973. New data on phase relations in the Cu–Fe–S system. Econ. Geol. 68, 443–454.

Craig, J., 1973. Pyrite–pentlandite assemblages and other low temperature relations in the Fe–Ni–S system. Am. J. Sci. 273A, 496–510.

Davies, R.M., Griffin, W.L., Pearson, N.J., Andrew, A.S., Doyle, B.J., O'Reilly, S.Y., Doyle, B.J., 1999. Diamonds from the Deep: Pipe DO-27, Slave Craton, Canada. Proc. 7th Int. Kimb. Conf. Red Roof Design cc, Cape Town, pp. 148–155.

Davis, W.J., Hegner, E., 1992. Neodymium isotopic evidence for the tectonic assembly of late Archean crust in the Slave Province, northwest Canada. Contrib. Mineral. Petrol. 111, 493–504.

Deines, P., Harris, J.W., 1995. Sulfide inclusion chemistry and carbon isotopes of African diamonds. Geochim. Cosmochim. Acta 59, 3173–3188.

Dromgoole, E., Pasteris, J., 1987. Interpretation of the sulfide assemblages in a suite of xenoliths from Kilbourne Hole and Potrillo Maar, New Mexico. In: Morros, E., Pasteris, J. (Eds.), Mantle Metasomatism and Alkaline Magmatism. Spec. Pap. - Geol. Soc. Am., pp. 25–46.

Drury, M.R., Van Roermund, H.L.M., 1989. Fluid assisted recrystallization in upper mantle peridotite xenoliths from kimberlites. J. Petrol. 30, 133–152.

Ertel, W., O'Neill, H.S.C., Dingwell, D.B., Spettel, B., 1996. Solubility of tungsten in a haplobasaltic melt as a function of temperature and oxygen fugacity. Geochim. Cosmochim. Acta 60, 1171–1180.

Fleet, M., Stone, W., 1990. Nickeliferous sulfides in xenoliths, olivine megacrysts and basaltic glass. Contrib. Mineral. Petrol. 105, 629–636.

Fleet, M.E., Stone, W.E., 1991. Partitioning of platinum-group elements in the Fe–Ni–S system and their fractionation in nature. Geochim. Cosmochim. Acta 55, 245–253.

Gaetani, G.A., Grove, T.L., 1997. Partitioning of moderately siderophile elements among olivine, silicate melt, and sulfide melt: constraints on core formation in the Earth and Mars. Geochim. Cosmochim. Acta 61, 1829–1846.

Gaetani, G.A., Watson, E.B., 2000. Open system behaviour of olivine-hosted melt inclusions. Earth Planet. Sci. Lett. 183, 27–41.

Garuti, G., Gorgoni, C., Sighinolfi, G.P., 1984. Sulfide mineralogy and chalcophile and siderophile element abundances in the Ivrea-Verbano mantle peridotites (Western Italian Alps). Earth Planet. Sci. Lett. 70, 69–87.

Gaul, O.F., Griffin, W.L., O'Reilly, S.Y., Pearson, N.J., 2000. Mapping olivine composition in the lithospheric mantle. Earth Planet. Sci. Lett. 182, 223–235.

Graham, S., Lambert, D.D., Shee, S.R., Smith, C.B., Reeves, S., 1999. Re–Os isotopic evidence for Archean lithospheric mantle beneath the Kimberley block, Western Australia. Geology 27, 431–434.

Griffin, W.L., Doyle, B.J., Ryan, C.G., Pearson, N.J., O'Reilly, S.Y., Davies, R., Kivi, K., van Achterbergh, E., Natapov, L.M., 1999. Layered mantle lithosphere in the Lac de Gras area, slave craton: composition, structure and origin. J. Petrol. 40, 705–727.

Griffin, W.L., Spetsius, Z.V., Pearson, N.J., O'Reilly, S.Y., 2002. In situ Re–Os analysis of sulfide inclusions in kimberlitic olivine: new constraints on depletion events in the Siberian lithospheric mantle. Geochem. Geophys. Geosyst. 3 (11), 1069 doi:10.1029/2001 GC000287.

Griffin, W.L., Graham, S., O'Reilly, S.Y., Pearson, N.J., 2003a. Lithosphere Evolution Beneath the Kaapvaal Craton: Re–Os systematics of Sulfides in Mantle-Derived Peridotites. Lithos 71, 215–241.

Griffin, W.L., O'Reilly, S.Y., Doyle, B.J., Pearson, N.J., Kivi, K., Malkovets, V., 2003b. Lithosphere Mapping Beneath the North American Plate. I: The Laurentian Continental Core. Proc. 8th Intl. Kimb. Conf., Victoria BC. Lithos (in press).

Grutter, H.S., Davis, W.J., Jones, A.G., 2000. Chemical and physical images of the central Slave Craton crust and mantle. Abstr. Pan-Lithoprobe Workshop II, Banff, pp. 32–33.

Hamlyn, P.R., Keays, R.R., 1986. Sulfur saturation and second-stage melts: application to the Bushveld platinum metal deposits. Econ. Geol. 81, 1431–1445.

Helz, R.T., 1977. Determination of the $P-T$ dependence of the first appearance of FeS-rich liquid in natural basalts to 20 kb. Abstr. EOS Trans. AGU, p. 533.

Irvine, G.J., Pearson, D.G., Kjarsgaard, B.A., Carlson, R.W., Kopylova, M.G., Dreibus, G., 2003. Evolution of the Lithospheric Mantle Beneath Northern Canada: a Re–Os Isotope and PGE Study of Kimberlite-Derived Peridotite Xenoliths from Somerset Island and a Comparison to the Slave and Kaapvaal cratons. Lithos 71, 461–480.

Jana, D., Walker, D., 1997. The influence of sulfur on partitioning of siderophile elements. Geochim. Cosmochim. Acta 61, 5255–5277.

Karup-Møller, S., Makovicky, E., 1995. The phase system Fe–Ni–S at 725 °C. Neues Jahrb. Mineral., Monatsh., 1–10.

Ketchum, J.W.F., Bleeker, W., 2001. Evolution of the Central Slave Basement Complex, Slave Craton, Canada: U–Pb constraints. Abstr. 11th Ann.V.M. Goldschmidt Conf., Abstr. #3148. LPI Contribution, vol. 1088.

Köhler, T.P., Brey, G.P., 1990. Calcium exchange between olivine and clinopyroxene calibrated as a geothermometer for natural peridotites from 2 to 60 kb with applications. Geochim. Cosmochim. Acta 54, 2375–2388.

Kullerud, G., Yund, R.A., Moh, G.H., 1969. Phase relations in the Cu–Fe–S, Cu–Ni–S, and Fe–Ni–S systems. Econ. Geol. Monogr. 4, 323–343.

Kusky, T.M., 1989. Accretion of the Archean Slave Province. Geology 17, 63–67.

Li, C., Barnes, S.-J., Maskovicky, E., Rose-Hansen, J., Makovicky, M., 1996. Partitioning of nickel, copper, iridium, rhenium, platinum, and palladium between monosulfide solid solution and sulfide liquid: effects of composition and temperature. Geochim. Cosmochim. Acta 60, 1231–1238.

Lodders, K., Palme, H., 1991. On the chalcophile character of molybdenum: determination of sulfide/silicate partition coefficients of Mo and W. Earth Planet. Sci. Lett. 103, 311–324.

Lorand, J.-P., 1987. Caractères mineralogiques et chimiques généraux des microphases du système Cu–Fe–Ni–S dans les roches du manteau supérieur: exemples d'hétérogénéités en domaine sub-continental. Bull. Soc. Geol. Fr. 4, 643–656.

Lorand, J.P., 1990. Are spinel lherzolite xenoliths representative of the abundance of sulfur in the upper mantle? Geochim. Cosmochim. Acta 54, 1487–1492.

Lorand, J.-P., Alard, O., 2001. Platinum-group element abundances in the upper mantle: new constraints from in situ and whole-rock analyses of Massif Central xenoliths (France). Geochim. Cosmochim. Acta 65, 2789–2806.

Lorand, J.P., Conquéré, F., 1983. Contribution à l'étude des sulfures dans les enclaves de lherzolite à spinelle des basaltes alcalins (Massif Central et Languedoc, France). Bull. Minéral. 106, 585–605.

Lorand, J.P., Ceuleneer, G., 1989. Silicate and base-metal sulfide inclusions in chromites from the Maqsad area (Oman ophiolite, Gulf of Oman): a model for entrapment. Lithos 22, 173–190.

Ludwig, K.R., 1999. Isoplot/Ex version 2.00; a geochronological toolkit for Microsoft ExcelSpecial Publication - Berkeley Geochronological Center, p. 46.

Makovicky, E., 2002. Ternary and Quaternary Phase Systems with PGE. In: Cabri, L.J. (Ed.), The Geology, Geochemistry, Mineralogy and Mineral Beneficiation of Platinum-Group Elements. Canadian Institute of Mining, Metallurgy & Petroleum, Montreal, pp. 131–178.

Mavrogènes, J.A., O'Neill, H.S.C., 1999. The relative effects of pressure, temperature and oxygen fugacity on the solubility of sulfide in mafic magmas. Geochim. Cosmochim. Acta 63, 1173–1180.

McDonough, W.F., Sun, S.-S., 1995. The composition of the Earth. Chem. Geol. 120, 223–253.

Mitchell, R.H., Keays, R.R., 1981. Abundance and distribution of gold, palladium and iridium in some spinel and garnet lherzolites—implications for the nature and origin of precious metal-rich intergranular components in the upper mantle. Geochim. Cosmochim. Acta 45, 2425–2442.

Noll, P.D.J., Newsom, H.E., Leeman, W.P., Ryan, J.G., 1996. The role of hydrothermal fluids in the production of subduction zone magmas: Evidence from siderophile and chalcophile trace elements and boron. Geochim. Cosmochim. Acta 60, 587–611.

Norman, M.D., Pearson, N.J., Sharma, A.L., Griffin, W.L., 1996. Quantitative analysis of trace elements in geological materials by laser ablation ICPMS: instrumental operating conditions and calibration values of NIST glasses. Geostand. Newsl. 20, 247–261.

Orberger, B., Xu, Y., Reeves, S.J., 1998. Platinum group elements in mantle xenoliths from eastern China. Tectonophys. 296, 87–101.

Padgham, W., Fyson, W., 1992. The Slave Province: a distinct craton. Can. J. Earth Sci. 29, 2072–2086.

Pattou, L., Lorand, J.-P., Gros, M., 1996. Non-chondritic platinum-group element ratios in the Earth's mantle. Nature 379, 712–715.

Peach, C., Mathez, E., Keays, R., 1990. Sulfide melt-silicate melt distribution coefficients for noble metals and other chalcophile elements as deduced from MORB: implications for partial melting. Geochim. Cosmochim. Acta 54, 3379–3389.

Pearson, N.J., Griffin, W.L., Doyle, B.J., O'Reilly, S.Y., van Achterbergh, E., Kivi, K., 1999. Xenoliths from kimberlite pipes of the Lac de Gras area, Slave Craton, Canada. 7th Intl. Kimb. Conf. Red Roof Design cc, Cape Town, pp. 644–658.

Pearson, N.J., Alard, O., Griffin, W.L., Jackson, S.E., O'Reilly, S.Y., Jackson, S.E., 2002. In situ measurement of Re–Os isotopes in mantle sulfides by laser ablation multicollector-inductively coupled plasma mass spectrometry: analytical methods and preliminary results. Geochim. Cosmochim. Acta 66, 1037–1050.

Pell, J., 1997. Kimberlites in the Slave Craton, Northwest Territories, Canada: a preliminary review. Proc. 6th Intl. Kimb. Conf.. Alberton Press, Novosibirsk, pp. 5–16.

Pouchou, J.L., Pichoir, F., 1984. A new model for quantitative X-ray microanalysis of homogeneous samples. Rech. Aerosp. 5, 13–38.

Poudjom Djomani, Y.H., O'Reilly, S.Y., Griffin, W.L., Doyle, B.J., 2003. Geophysical analysis of the lithosphere beneath the Slave craton. Abstr. 8th Intl. Kimb. Conf., Victoria BC.

Puchtel, I., Humayun, M., 2000. Platinum group elements in Kostomuksha komatiites and basalts: Implications for oceanic crust recycling and core–mantle interaction. Geochim. Cosmochim. Acta 64, 4227–4242.

Rama Murthy, V., Hall, H.T., 1972. The origin and chemical composition of the Earth's core. Phys. Earth Planet. Inter. 6, 123–130.

Richardson, S.H., Shirey, S.B., Harris, J.W., Carlson, R.W., 2001. Archean subduction recorded by Re/Os isotopes in eclogitic sulfide inclusions in Kimberley diamonds. Earth Planet. Sci. Lett. 191, 257–266.

Roy-Barman, M., Wasserburg, G.J., Papanastassiou, D.A., Chaussidon, M., 1998. Osmium isotopic compositions and Re–Os concentrations in sulfide globules from basaltic glass. Earth Planet. Sci. Lett. 154, 331–347.

Schaefer, B.F., Turner, S., Parkinson, I., Rogers, N., Hawkesworth, C., 2002. Evidence for recycled Archaean oceanic mantle lithosphere in the Azores plume. Nature 420, 304–307.

Smoliar, M.I., Walker, R.J., Morgan, J.W., 1996. Re–Os ages of Group IIA, IIIA, IVA, and IVB iron meteorites. Science 271, 1099–1102.

Sobolev, N., Efimova, E., Pospelova, L., 1981. Native iron in Yakutian diamonds and its paragenesis. Geol. Geofis. 22, 25–28 (in Russian).

Suzuki, T., Akaogi, M., 1995. Element partitioning between olivine and silicate melt under high pressure. Phys. Chem. Miner. 22, 411–418.

Szabó, C., Bodnar, R.J., 1995. Chemistry and origin of mantle sulfides in spinel peridotite xenoliths from alkaline basaltic lavas, Nógrád-Gömör volcanic field, Northern Hungary and Southern Slovakia. Geochim. Cosmochim. Acta 59, 3917–3927.

Thompson, J.F.H., Barnes, S.J., 1984. The distribution of nickel and iron between olivine and magmatic sulfides in some natural assemblages. Can. Mineral. 22, 55–66.

Walker, R.J., Nisbet, E., 2002. ^{187}Os isotopic constraints on Archean mantle dynamics. Geochim. Cosmochim. Acta 66, 3317–3325.

Walker, R.J., Carlson, R.W., Shirey, S.B., Boyd, F.R., 1989. Os, Sr, Nd, and Pb isotope systematics of southern African peridotite xenoliths: implications for the chemical evolution of subcontinental mantle. Geochim. Cosmochim. Acta 53, 1583–1595.

Walker, R.J., Morgan, J.W., Horan, M.F., Czamanske, G.K., Krogstad, E.J., 1994. Re–Os isotopic evidence for an enriched-mantle source for the Noril'sk-type, ore-bearing intrusions, Siberia. Geochim. Cosmochim. Acta 58, 4179–4197.

Walker, R.J., Morgan, J.W., Horan, M.F., 1995. Osmium-^{187} enrichments in some plumes: a consequence for core–mantle interaction? Science 269, 819–822.

Walker, R.J., Morgan, J.W., Hanski, E., Smolkin, V.F., 1997. Re–Os systematics of early proterozoic ferropicrites, pechenga complex, NW Russia: evidence for ancient ^{187}Os-enriched plumes. Geochim. Cosmochim. Acta 61, 3145–3160.

Wendlandt, R., 1982. Sulfide saturation of basalt and andesite melts at high pressures and temperatures. Am. Mineral. 67, 877–885.

Westerlund, K.J., Shirey, S.B., Richardson, S.H., Gurney, J.J., Harris, J.W., 2003. Re–Os isotope systematics of peridotitic diamond inclusion sulfides from the Panda kimberlite, Slave craton. Abstr. 8th Intl. Kimb. Conf., Victoria BC.